SAInt – A novel quasi-dynamic model for assessing security of supply in coupled gas and electricity transmission networks

Pambour, Kwabena Addo; Cakir Erdener, Burcin; Bolado-Lavin, Ricardo; Dijkema, Gerhard P.J.

Published in:
Applied Energy

DOI:
10.1016/j.apenergy.2017.05.142

Publication date:
2017

Applied Energy 203 (2017) 829–857

Contents lists available at ScienceDirect

Applied Energy

journal homepage: www.elsevier.com/locate/apenergy

SAInt – A novel quasi-dynamic model for assessing security of supply in coupled gas and electricity transmission networks

Kwabena Addo Pambour [a], Burcin Cakir Erdener [b], Ricardo Bolado-Lavin [c,*], Gerard P.J. Dijkema [a]

[a] University of Groningen, Faculty of Science and Engineering, Energy and Sustainability Research Institute Groningen (ESRIG), Nijenborgh 6, 9747 AG Groningen, The Netherlands
[b] European Commission, Joint Research Centre, Directorate (C) for Energy, Transport and Climate, Via Enrico Fermi 2749, I - 21027 Ispra, VA, Italy
[c] European Commission, Joint Research Centre, Directorate (C) for Energy, Transport and Climate, Westerduinweg 3, NL-1755 ZG Petten, The Netherlands

HIGHLIGHTS

- Transient gas model combined with augmented economic dispatch model.
- Solution of combined model in single simulation time frame and environment.
- Development of parameters to quantify impact of disruptions on security of supply.
- Implementation into novel simulation tool SAInt for assessing security of supply.
- Detailed information on timing and propagation of contingencies.

GRAPHICAL ABSTRACT

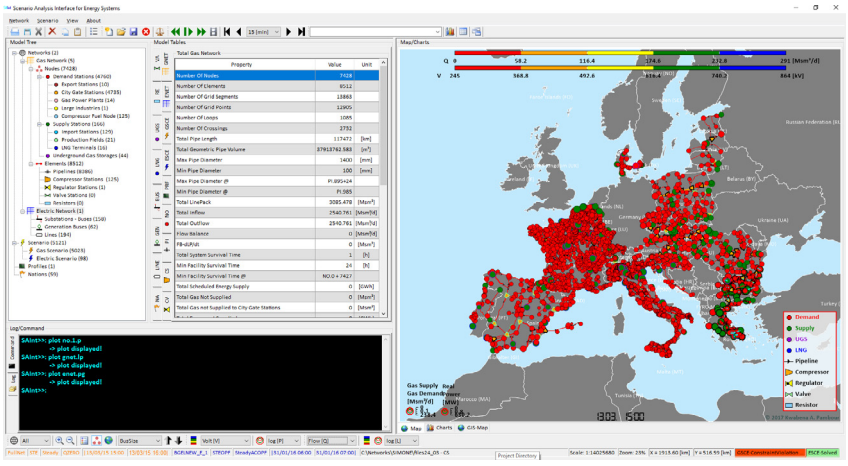

ARTICLE INFO

Article history:
Received 3 January 2017
Received in revised form 16 May 2017
Accepted 22 May 2017

Keywords:
Combined power gas simulation
Power gas interdependence
Security of supply
Contingency analysis
AC-optimal power flow
Transient hydraulic gas simulation

ABSTRACT

The integration of renewable energy sources into existing electric power systems is connected with an increased interdependence between natural gas and electricity transmission networks. To analyse this interdependence and its impact on security of supply, we developed a novel quasi-dynamic simulation model and implemented it into the simulation tool `SAInt` (Scenario Analysis Interface for Energy Systems), the first published software application that allows the combined simulation of gas and electric power systems in a single time frame and simulation environment. The model is composed of a transient hydraulic simulation model for the gas system and an augmented AC-Optimal Power Flow model for the electric power system, which includes a model for dispatchable power system loads and considers time transitional constraints, such as the ramp rate and the start-up time of generation units. Both models take into account the control and constraints of the most relevant facilities present in both systems. The bidirectional interconnection between both systems is considered and established by coupling equations describing the fuel gas offtake for power generation in gas fired power plants, and the electric power supply to LNG terminals and electric driven compressors in gas compressor stations. The resulting system of equations for the combined model are solved in a single simulation time frame. In order to quantify the impact of different contingencies on the operation of the combined system, a number of security of supply parameters are proposed, which can be utilised to compare the impact of different contingencies on

* Corresponding author.
E-mail addresses: kwabena.pambour@gmail.com (K.A. Pambour), burcincakir55@gmail.com (B. Cakir Erdener), ricardo.bolado-lavin@ec.europa.eu (R. Bolado-Lavin), g.p.j.dijkema@rug.nl (G.P.J. Dijkema).

http://dx.doi.org/10.1016/j.apenergy.2017.05.142
0306-2619/

Nomenclature

Abbreviations

AC	alternating current
CCH	constraint and control handling of controlled facilities in gas systems
CCGT	combined cycle gas turbine
CBE	cross border export
CBI	cross border import
CEI	critical energy infrastructures
CGS	city gate station
DC	direct current
DTA	dynamic time step adaptation method
ED	economic dispatch
EDCS	electric driven compressor station
ENS	energy not supplied
ENSTSP	energy not supplied per time span
ESUB	subsystem of electric network
EU	european union
GFPP	gas fired power plant
GNS	gas not supplied
GSUB	subsystem of gas network
GT	conventional gas turbine
IND	large industrial customer directly served from the gas or power transmission grid
KKT	Karush Kuhn Tucker optimality condition
LDS	local distribution system
LNG	liquefied natural gas
NGTS	national gas transport system
P2G	power to gas
PENS	percentage of energy not supplied
PDE	partial differential equation
PDIPM	primal dual interior point method
OPF	optimal power flow
SAInt	Scenario Analysis Interface
SCO	simulation control object
SNG	synthetic natural gas
SVT	survival time
RA	reserve allocation
RES	renewable energy sources
TSO	transmission system operator
TSP	time span of energy not supplied
UC	unit commitment
UGS	underground gas storage

Mathematical symbols

$\mathbf{A}$	node branch incidence matrix
A	cross-sectional area
a	transformer tap ratio
b	line charging susceptance
c_0, c_1, c_2	coefficients of cost function
c	speed of sound
D	inner pipe diameter
e	Euler's number
$\mathbf{F}$	residual vector
f	electric driver factor
FB	flow balance (total gas inflow minus total gas outflow)
g	gravitational acceleration
GCV	gross calorific value
HR	heat rate
I_f	electric current injection at from bus
I_t	electric current injection at to bus
$INVMAX$	maximum working gas inventory
j	imaginary number
k_0, k_1, k_2	coefficients of coupling equation for LNG terminals
k	iteration step
k_c	constraint handling iteration step
L	nodal load (vector), Lagrange function
L^{GFPP}	fuel gas offtake for power generation at GFPPs
l	pipe length
LP	line pack
M	number of pipe section
n	simulation time point
N	number of gas nodes
N_b	number of buses
N_{CS}	number of compressor stations
N_g	number of power generation units
N_{GFPP}	number of GFPPs
N_{iq}	number of inequality constraints
N_l	number of transmission lines and transformers
N_{LNG}	number of LNG terminals
P_D	active power demand
P_D^{CS}	power demand of compressor stations
P_D^{set}	scheduled electric power demand at load buses
P_G	active power generation
$\mathbf{P_G}$	vector of active power generation
p	gas pressure (vector)
p_1	inlet pressure
p_2	outlet pressure
$PIMIN$	minimum inlet pressure
$PMAX$	maximum nodal pressure
p_n	pressure at reference conditions
Res	residual
$POSET$	outlet pressure set point
$POMAX$	maximum outlet pressure
$PRMAX$	maximum pressure ratio
$PWMAX$	maximum available driver power
$POWD$	driver power
Q	gas flow rate, reactive power
$\mathbf{Q_G}$	vector of reactive power generation
$QMAX$	maximum flow rate
$QREG$	regasification rate
R	gas constant, line resistance
t	time, complex transformer tap
t_a	point in time at which a facility is affected by a disruption
t_d	point in time at which a disruption event occurs
t_n	point in time
Δt	time step
T	temperature
T_n	reference temperature
T_s	start up time
T_d	shut down time
v	gas velocity
V	complex bus voltage
$\mathbf{V}$	vector of complex bus voltage
$\mathbf{V_m}$	vector of complex bus voltage magnitudes
$\|V\|$	bus voltage magnitude
V_i	nodal volume
X	line reactance
x	pipeline coordinate
$\mathbf{X}$	vector of decision variables
Δx	pipe segment length
Y	line admittance
$\mathbf{Y_{bus}}$	bus admittance matrix
Z	compressibility factor, impedance

Greek symbols

α	inclination
α, β, γ	coefficients of heat rate curve
α_p	primal truncation factor for Newton update
α_d	dual truncation factor for Newton update
γ	perturbation factor for cost function of slack variables

δ	voltage angle
Δ	vector of bus voltage angles; deviation
ϵ	residual tolerance
ϵ_{svt}	survival time tolerance
ζ	scale factor for newton update
η	dynamic viscosity
η_{ad}	compressor adiabatic efficiency
η_m	driver efficiency
η_T	thermal efficiency
κ	isentropic exponent
λ	friction factor, (vector of) Lagrange multipliers for equality constraints, priority factor for power system loads
μ	(vector of) Lagrange multipliers for inequality constraints
π	slope of penalty function for dispatchable power system loads
ϕ	transformer phase shift angle
ρ	gas density
ρ_n	gas density at reference conditions
σ	scale factor for average primal dual distance
ξ	scale factor for *pi*
ω_r	ramp rate of a power plant

Physical units

[sm^3]	standard cubic metres (line pack, inventory)
[ksm^3/h]	thousands of standard cubic metres per hour (gas flow rate)
[Msm^3]	millions of standard cubic metres (line pack, inventory)

security of supply and the effectiveness of countermeasures to mitigate this impact. The capabilities of the combined model and the functionality of the simulation tool `SAInt` are demonstrated in a case study of a sample gas and power transmission system. Results indicate how the combined simulation of gas and electric power systems can give insight into important and critical information, such as the timing and propagation of contingencies cascading from one system to the other or the grace period to react to these contingencies. Such information can contribute to improving the coordination between gas and power transmission system operators in the event of a disruption, thus, increasing the resilience and the level of security of supply in the combined energy system. The information provided by the combined model cannot be obtained by the traditional co-simulation approach, where both systems are solved in different time frames. Furthermore, the studies stress the importance of using transient gas simulation models for security of supply analysis instead of steady state models, where the time evolution of gas pressure and linepack are not reflected appropriately.

1. Introduction

The ongoing integration of renewable energy sources (RES) into existing energy supply systems is connected with an increased coupling between natural gas and electric power transmission systems.

On the power side, the installation of variable RES, such as wind and solar, is increasing, which require flexible and reliable back up generation units with short start-up and shut down times and large ramping rates in order to provide the flexibility needed in the electricity system to cover the variability and uncertainty provided by wind and solar power. Gas fired power plants (GFPP) connected to gas and electricity networks, which are known for their reliability, short start-up time and shut down time can provide such flexibility to the electric power system [1].

On the gas side, an increased use of electric power to operate facilities in the gas system such as liquefied natural gas (LNG) terminals and electric driven compressors installed in gas compressor stations and underground gas storage (UGS) facilities, can be noticed [2]. Electric drivers outperform traditional gas turbines with a higher mechanical efficiency, lower maintainance costs and less impact on the environment [3].

In addition to these interconnections, the power to gas (P2G) technology will significantly contribute to the coupling between both systems [4,5], where excess electric energy production (e.g. during variable RES curtailment) is used in an electro-chemical process to produce hydrogen and synthetic natural gas (SNG), which can be injected and stored in gas pipelines or UGS facilities for later use at peak electricity demand periods. As more P2G facilities are installed, the dependence of electric power systems on gas network systems as a provider for energy storage will increase.

These developments stress the need to

(1) examine the depth and scope of these interdependencies,
(2) how they may affect the operation of both systems and
(3) how to proactively approach the bottlenecks and challenges that may emerge.

The traditional co-simulation approach, where the physical equations for the gas and electric power system are solved in independent time frames [6–10] and/or a steady state model is used for the gas system [8–12], can only give qualitative information on how a contingency may affect security of supply in coupled gas and electric power systems. For instance, a steady state approach for the gas system cannot quantify appropriately the time evolution of the quantity of gas stored in pipelines, also referred to as linepack, which is a key indicator [6] for how much flexibility the gas system can provide to GFPPs for electric power generation (e.g. available ramping capacity for fuel gas extraction at start-up of spinning reserves, which have to deliver electric energy within 10–30 [min] in case of a contingency [13]).

Furthermore, the co-simulation approach cannot estimate accurately the grace period for gas and power transmission system operators (TSOs) to coordinate and deploy counter measures to mitigate a contingency. In order to examine the issues raised in (1)–(3) in a quantitative way, a dynamic model of the coupled gas and electric power system is needed, that can reflect appropriately how disruptions triggered in one system propagate to the other system and affect the operation of facilities in both systems. This will allow gas and power system stakeholders to suggest modifications, that may help prevent and/or mitigate the consequences

of disruptions. Some of these modifications, that can be implemented are, for instance:

(a) The curtailment of gas and electric power loads at specific locations and times to reduce the stress on the system and to prevent insufficient pipeline pressures
(b) The installation of UGS facilities at strategic locations to increase the flexibility to react to loss or shortage of gas supply
(c) The increase of withdrawal capacity of existing UGS facilities,
(d) The shut-down of specific power plants to maintain the operation of the system in degraded mode,
(e) The expansion of the network to increase transmission capacities and line pack
(f) The availability of reverse flow at cross-border-points to increase the flexibility and resilience of the gas system

Recent publications [4,6,7,13–19] demonstrate the growing interest in analysing the interconnection between gas and electric power systems. While most publications address the issue with a steady state model for the gas system integrated into a co-simulation environment, where both systems are solved in independent time frames [7–9,11,19,20], there is currently no publication addressing the issue with a combined model that includes the full set of the following important model requirements for assessing security of supply in interconnected gas and electric power systems:

(i) Dynamic model for the gas pipeline system (i.e. imbalance between gas supply and gas demand resulting in fluctuations in linepack), in order to reflect appropriately the changes in pressure and linepack.
(ii) AC model for the electric power system, in order to capture line losses, reactive power flow, voltage levels etc., which are neglected in DC models.
(iii) Simultaneous solution of the physical equations and coupling equations for the interconnected gas and electric power system for each simulation time step, in order to capture the direct impact of control changes or disruptions originating from one system and cascading to the other system.
(iv) Consideration of the bidirectional interconnection between both systems (i.e. gas offtake for power generation in GFPPs and power supply to EDCS and LNG terminals), in order to give a full picture of the interdependence between both systems.
(v) Generic sub models for the most important gas and power system facilities (e.g. compressor stations, UGS, LNG terminals, generation units, electric substations etc.) and their technical and legal constraints (e.g. pressure limits, operating envelope of compressors, voltage limits, generator capability curves, transmission line capacity limits etc.), in order to reflect adequately the flexibility and operation of both systems in scenarios, where both system operate close to their limits.
(vi) Possibility to implement conditional control changes, i.e. changing the set points in one system in respect to the conditions in the other system (e.g. the start up of a GFPP for power generation depends on the available linepack and pressure in the gas system), in order to model the coordination between both systems and how they may improve the combined operation.
(vii) Estimation of consequences of supply disruptions, in order to quantify how disruptions affect security of supply and to analyse the effectiveness of countermeasures to mitigate the impact of disruptions.

Studies in the literature that use combined simulation to examine the interconnection between gas and power systems for planning purposes mainly focus on single or multi-time period operational optimisation methods based on steady state conditions [7,16,17,21–24]. In [22], the authors investigate the short-term optimal operation of the integrated gas and electricity network with wind power and P2G facilities. The authors use a security-constraint bi-level ED model with an objective function that minimizes the day ahead costs of electricity and natural gas consumption, respectively. In [23], a multi-stage co-planning model is developed to identify the optimal expansion planning of integrated gas and electricity networks. In [16], a coupled steady state model is proposed to analyse the mitigation effects of integrated gas and electricity systems using a succession of steady states approach with time varying power demand and wind generation profiles. The authors use a steady state gas system model to address a dynamic problem. In [7], a unit commitment and ED model that considers the technical characteristics of power generation units is proposed. The authors include an energy flow model for the gas system taking into account pressure constraints. An interval optimisation strategy for short-term scheduling of coupled gas and electricity system is proposed in [24], where demand response and wind uncertainty are considered. In [17], the authors propose a multi-linear probabilistic energy flow framework for investigating the impacts of uncertainties on the operation of both systems using Monte-Carlo simulations. The authors use a combined steady state model for describing the gas and electric power system. Moreover, they consider the bi-directional coupling between both systems taking into account the voltage and frequency dependency of electric power system loads. Additional stochastic optimisation models are proposed in [11,25,26] in order to address the uncertainties of the integrated gas and electricity networks.

In the above studies, the dynamic behaviour of the gas system is neglected, which, however, is relevant when studying the combined operation of gas and electric power systems [6,13]. The time evolution of linepack determines the level of flexibility the gas system can provide to the electric power system. In a steady state gas model the time derivative of the linepack is inherently zero, since total gas inflow and outflow are at equilibrium. Thus, the time evolution of the linepack cannot be captured appropriately by steady state gas models.

To account for this aspect, researchers have developed models for combined optimisation of gas and electricity networks considering the dynamics in gas pipeline systems [6,13,18,27,28]. In [27], a multi-time period optimisation model is proposed for analysing the coupling between the gas and power system network in Great Britain. The authors model key gas system facilities such as compressor stations and UGS facilities and their constraints. The power system model used in the study is based on a simplified DC-OPF model, where important power system constraints, such as thermal capacity limits of transmission lines and reactive power limits of generation units are disregarded. Moreover, the authors consider the ramping limits of generation units, but neglect their start-up and shut down time limits, which may restrict the availability and flexibility of these units. Furthermore, the bi-directional coupling between the gas and electric power system is neglected, since only the coupling through GFPPs is considered. In [28], the authors present a detailed optimal control model to capture spatio-temporal interactions between gas and electricity systems. The proposed model couples a dynamic gas model with an economic dispatch model for the power grid in order to investigate the economic and flexibility gains resulting from coordinating the dispatch of both systems. Similar to the previous study [27] the power system model is based on a simplified DC model, which is connected with the limitations explained above.

In [18,13], the authors introduce a coupled optimisation model for the combined simulation of gas and electric power systems, where both systems are coupled through gas fired power plants solely. The model is intended to assist gas and power TSOs in coordinating the scheduling of gas offtakes for power generation in GFPPs. Similar to the other studies the authors use a DC-OPF approach to model the electric power system. In a previous publication [15], we proposed a coupled multi-time period model for simulating the operation of gas and electric power systems by solving the physical equations and coupling equations in a single time frame and for multiple simulation time steps. We used a transient hydraulic model for the gas system and a steady state model for the electric power system based on AC-power flow (AC-PF), with a distributed slack bus approach for balancing power demand and power losses. By assigning a participation factor to each GFPP, we used the flexibility offered by these units to balance the electric power system. While the model is able to capture basic interdependencies between both systems, its practical use is limited, since key electric power system constraints such as maximum transmission line capacities, upper and lower limits on power generation and voltages are not considered. In addition, the distributed slack bus approach does not reflect adequately the real time power dispatch in electric power system operation, which is typically scheduled by solving a unit commitment (UC), economic dispatch (ED) and reserve allocation (RA) problem. These problems are typically described by mixed integer linear programs or (non)-linear constrained optimisation models [13].

In this paper, we cover the gaps in the available literature by extending the simulation tool *SAInt* (Scenario Analysis Interface for Energy Systems) [14,15,29] by a novel combined quasi-dynamic model composed of a transient hydraulic simulation model for the gas system, which considers the constraints and control of the most important facilities in the gas system, such as compressor stations and UGS facilities, and a steady state model for the electric power system based on AC-optimal power flow (AC-OPF), where the operational costs and key electric power system constraints such as transmission line capacity limits, active and reactive power generation limits and upper and lower limits on bus voltage magnitudes are considered. The bi-directional coupling between both systems is established by synchronising the fuel gas offtake from the gas system for power generation in GFPP and the electric power supply to electric driven compressors installed in gas transport systems. Moreover, the power supply to LNG terminals is also modelled as an additional gas system dependence on the electric power system.

The scope of the proposed model is primarily on the technical operation of the integrated energy system in a contingency scenario, assuming that market based measures have been fully exploited but were insufficient to mitigate the impact of a disruption. Therefore, aspects related to the energy market are only considered partly in this studies.[1] Furthermore, in order to reduce the complexity of the combined model, we do not consider the dynamic behaviour of the electric power system, which may have an influence on the combined operation of both systems. We assume that the automatic generation control (AGC) system is capable of returning the power system to a balanced and stable steady state within a short time frame (less than 5 [min]) after a disturbance [30].

To the best of our knowledge, there is currently no commercial or open source simulation software on the market, that allows the coupled simulation of gas and electric power systems in a single time frame and simulation environment. Thus, *SAInt* is the first published software tool to offer this type of functionality.

The model presented in this paper and implemented into *SAInt* is intended to assist governments, gas and power TSOs, regulatory agencies and researchers to address the challenges connected with the ongoing transformation of critical energy infrastructures (CEIs). In particular, *SAInt* can be used to examine potential threats to security of energy supply and to develop strategies to prevent and mitigate the consequences of undesired disruption events in multi-vector energy systems with high penetrations of variable RES. Moreover, the capability of *SAInt* to quantify the impact of a disruption on security of supply can be utilised to perform a full risk assessment of CEIs as postulated by EU Regulation 994/2010 [31], which involves, the identification of critical scenarios, the probability of their occurrence and the impact of the identified scenarios on security of supply, which can be estimated by *SAInt* [29].

To achieve these goals, the paper follows the following structure. In Section 2.1 and 2.2, we develop the mathematical models for the gas and electric power system independently. In Section 2.3, we discuss the interconnections between both systems and derive the coupling equations for the combined system. Next, we describe the algorithm for solving the resulting system of equations for the combined energy system, followed by the definition of parameters to evaluate and quantify the impact of disruptions on security of energy supply in Section 3. Finally in Section 4, the functionality of the simulation tool and the capability of the implemented simulation model are demonstrated in a case study of a sample combined gas and electric power transmission network.

2. Methodology

The operation of gas and electric power systems is increasingly interdependent, due to an increased physical interconnection between the facilities installed in both systems. A change in one system may propagate to the other system and even back to the triggering system. For instance, an increase in power generation from a GFPP, will cause the gas offtake from the gas grid to increase. This, in turn, may result in an increased power offtake of electric driven compressor stations (EDCS) to recover the pressure and line pack level in the area affected by the gas offtake. The additional power offtake, again, will have to be balanced by the power generation units including GFPPs, by increasing the power output. This cycle may continue until an equilibrium dynamic state is reached. The equilibrium state in such a bidirectionally coupled system cannot be captured appropriately with the traditional co-simulation approach, where both systems are analysed in independent time frames, rather an integrated simultaneous solution of the physical equations describing the operation of the coupled multi-vector energy system at each simulation time step is needed.

The first challenge that arises when modelling the coupled power-gas system is to find a simulation model that describes the dynamic behaviour of the individual systems appropriately.

The dynamics in gas transport systems, for instance, are much slower than the ones in electric power systems. Electricity travels almost instantaneously (with speed of light $3 \cdot 10^8$ [m/s]) and cannot be stored economically in large quantities in current electric power systems[2] [8]. In case of a disruption, the response time of the electric power system is quite fast and basically the transmission line flows satisfy the steady-state algebraic equations. On the contrary, natural gas pipeline flow is a much slower process, with gas flow velocities typically below 10 [m/s] and the propagation of pressure and flow changes around 350 [m/s] (typical value for the speed

[1] Operational costs for each power plant are considered.

[2] With the only exception of hydraulic pumping power stations, whose availability is very much limited in a significant number of countries.

of sound), resulting in a longer response time in case of a large fluctuation. In particular, high-pressure transmission pipelines have much slower dynamics due to the large sums of natural gas stored in the pipelines.

In order to consider the different characteristics of both systems, we propose a transient model for the gas system and a steady state AC model for the electric power system.

The steady state of an electric power system is described by the active and reactive power balance equations, which are typically solved with a power flow model, where the power system loads at load buses and voltage magnitude and active power control settings at generation buses are prescribed as inputs except for one generation bus, which serves as a slack bus to balance power system loads and line losses. The constraints of the power system are not included in the power flow model, but are checked after each power flow calculation. In case a constraint violation is detected the control settings for the load and generation buses are adjusted manually and the power flow model is recomputed. The adjustments are made based on experience or a predefined protocol. This iterative process is repeated until a feasible solution that satisfies all constraints is obtained. The advantage of this approach is that the feasible operating region of the power system is kept as wide as the constraints permit and the obtained solution is a realistic state of the network. The disadvantage, however, is that the iterative solution process may be time consuming and the final solution obtained may not provide the most economical power dispatch schedule for the given constraints. Moreover some constraints of the power system, such as the thermal capacity limits of transmission lines are difficult to implement mathematically, since the corresponding variables (current, apparent and active power flows in lines) are not given explicitly in the power balance equations. For security of supply studies, where the power system operates close to its limits it is extremely important to reflect appropriately the constraints of the power system at reasonable computational costs. Therefore, we propose an optimal power flow (OPF) model, which determines in a single simulation run the most economical control settings for load and generation buses and at the same time respects key power system constraints such us thermal capacity limits of transmission lines, reactive and active power and ramping limits of generation units and voltage limits of load buses. The solution obtained by the AC-OPF model is an ideal steady state of the power system network based on the objective function and constraints provided to the model.

The proposed gas and power system model are coupled to a combined simulation model by defining coupling equations reflecting the physical interlink between both systems at each simulation time step.

In the following, we derive the gas and electric power system models independently. Next, we describe mathematically the most important interconnections between both systems and integrate the coupling equations into the individual models. Finally, we propose a method for solving the resulting system of equations describing the operation and interdependencies of the combined gas and electric power system.

2.1. Gas system model

A gas network can be described by a directed graph $G = (V, E)$ composed of nodes V and branches E. Facilities with an inlet, outlet and flow direction are modelled as branches, while connection points between these branches as well as entry and exit stations are represented by nodes. Branches, in turn, can be distinguished between active and passive branches. Active branches represent controlled facilities, which can change their state or control during operation, such as compressor stations, regulator stations and valves, while passive branches represent facilities or components

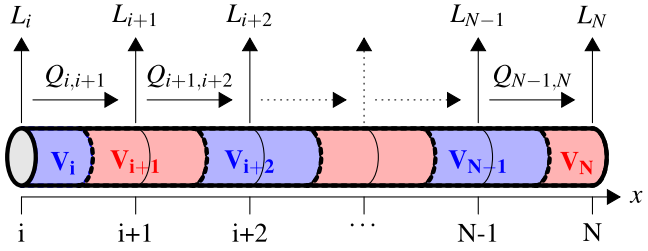

Fig. 1. Pipeline discretization.

which state is fully described by the physical equations derived from the conservation laws, such as pipelines and resistors.[3]

The gas flow in transport pipelines is inherently dynamic. Supply and demand are constantly changing and the reactions of the system to these changes are relatively slow, due to the small flow velocities (typically below 10 [m/s]) and the large volume of gas stored in transport pipelines.

The dynamic behaviour of a gas system is predominately determined by the gas flow in pipelines. In general, a gas pipeline has four basic properties, namely, capacity (i.e. the ability to store a certain volume of gas, which depends on the geometric volume and the maximum design pressure of the pipeline), resistance (i.e. force acting opposite to the gas flow direction, caused by friction between the gas and the inner walls of the pipeline), inertia (force acting opposite to the gas flow acceleration) and gravity (gravitational force acting on the gas volume in sloped pipelines). Capacity and resistance are the predominant properties, while in most cases gravity and inertia play a secondary role. A gas pipeline can be segmented into N nodal control volumes V_i and M pipe sections (see Fig. 1), assuming each section inherits a fraction of the basic properties of the original pipeline (e.g. pipe length l, diameter D, roughness r and inclination α). According to the mass conservation law, the gas density ρ_i of a nodal control volume V_i may change in time, if there is an imbalance between total gas inflow and outflow to V_i. If we assume isothermal[4] flow conditions, the mass conservation law can be expressed by the following integral form of the continuity equation:

$$\frac{V_i}{\rho_n c^2}\frac{dp_i}{dt} = \sum_{j=1}^{k} a_{ij} Q_{ij} - L_i \tag{1}$$

$$c^2 = \frac{p}{\rho} = ZRT, \quad V_i = \frac{\pi}{8}\sum_{j=1}^{k} D_{ij}^2 \Delta x_{ij} \tag{2}$$

The continuity equation can be expressed for each nodal control volume in the network, thus, we obtain N set of equations with $N + M$ unknown state variables (p_i, Q_{ij}). If we perform an implicit time integration on this set of equations for a time step $\Delta t = t_{n+1} - t_n$ and sort the equation in terms of known variables

[3] Any device that causes a local pressure drop, such as filters, scrubbers, heaters, metering devices can be modelled as a resistor. The difference between a resistor and a pipe is that the pipe has the capability to store a specific quantity of gas referred to as linepack.

[4] Isothermal flow means the gas temperature T is constant in time and space and equal to the ground temperature. Hence, the time and space derivatives of the temperature can be neglected. In reality the gas temperature may change along the pipeline due to the Joule-Thompson effect (i.e. temperature drop of real gases caused by an expansion of the gas) and heat exchange between the gas and the environment. While the impact of these changes on the gas pressure is marginal [32], neglecting temperature changes can have an influence on the value of the linepack. However, to capture this influence adequately requires a good knowledge of the heat resistance of the ground and the heat transfer coefficients between the gas, the pipeline and the ground, which is typically not available. Thus, the assumption of isothermal flow is reasonable and well accepted in the scientific community [33–37].

at time t_n (right hand side) and unknown variables at time t_{n+1} (left hand side), we obtain the following set of linear finite difference equations for the total network:

$$\Phi p^{n+1} - \mathbf{A}Q^{n+1} + L^{n+1} = \Phi p^{n} \tag{3}$$

$$\Phi = diag\{\phi_1, \phi_2, \ldots, \phi_n\}, \quad \phi_i = \frac{V_i}{\rho_n c^2 \Delta t} \tag{4}$$

In order to close and solve eq. (3) for the entire network including non-pipe facilities, M additional independent equations are needed, which correlate the state variables p_i, Q_{ij} and L_i. These equations are provided by the pressure drop equation for each pipe section and the equations describing the control modes and constraints of non-pipe facilities, such as compressor stations, UGS facilities and LNG terminals.

The pressure drop equation for a pipe section is derived from the law of conservation of momentum, which yields the following momentum equation:

$$\underbrace{\frac{\partial(\rho v)}{\partial t}}_{\text{inertia}} + \underbrace{\frac{\partial(\rho v^2)}{\partial x}}_{\text{convective term}} + \underbrace{\frac{\partial p}{\partial x}}_{\text{pressure}} + \underbrace{\frac{\lambda \rho v|v|}{2D}}_{\text{friction}} + \underbrace{\rho g sin\alpha}_{\text{gravity}} = 0 \tag{5}$$

Eq. (5) can be reduced to the following non-linear hyperbolic partial differential equation (PDE), if we assume isothermal flow conditions and neglect the convective term.[5]

$$\frac{\partial p}{\partial x} = -\frac{\rho_n}{A}\frac{\partial Q}{\partial t} - \frac{\lambda \rho_n^2 c^2}{2DA^2 p}|Q|Q - \frac{g \sin\alpha}{c^2}p \tag{6}$$

Eq. (6) can be discretized using a fully implicit finite difference scheme, where the state variables (p, Q) and their partial derivatives are approximated as follows:

$$\frac{\partial U}{\partial t} = \frac{U_i^{n+1} - U_i^n}{\Delta t}, \quad \frac{\partial U}{\partial x} = \frac{U_{i+1}^{n+1} - U_i^{n+1}}{\Delta x}, \quad U = \frac{U_{i+1}^{n+1} + U_i^{n+1}}{2} \tag{7}$$

The resulting non-linear finite difference equation for each pipe section is linearised in each step of the iterative solution process using the solution from the preceding time step n as an initial guess.

The quantity of gas stored in gas pipelines at simulation time t_n, which is also referred to as linepack $LP(t_n)$ is an important parameter for the flexibility the gas network can provide to GFPPs in the electricity network. The start-up of a GFPP or the ramping of an active GFPP depends on the availability of sufficient fuel gas pressure and linepack in the upstream hydraulic area. A gas network can be separated into hydraulic areas, which are controlled by active elements. A hydraulic area is a subsystem of interconnected pipelines, which are bounded by controlled facilities, such as compressor stations, regulator stations and closed valves. The linepack in a gas pipeline can be expressed as follows [14]:

$$LP(t_n) = \frac{A}{\rho_n \cdot c^2}\int_{x=0}^{x=\Delta x} p(x, t_n)\, dx = \frac{\Delta x\; p_m(t_n)\; A}{\rho_n \cdot c^2} \tag{8}$$

with

$$p_m(t_n) = \frac{2}{3}\frac{p_1(t_n)^2 + p_1(t_n)\cdot p_2(t_n) + p_2(t_n)^2}{p_1(t_n) + p_2(t_n)} \tag{9}$$

where p_m is the mean pressure in the pipe section and p_1 and p_2 are the inlet and outlet gas pressure, respectively. We account for the availability of linepack for operating GFPPs by assigning conditional expressions for the operation of a GFPP, which we explain further in Sections 3 and 4.

The integration of non pipe facilities such as compressor stations, UGS facilities and LNG terminals into the gas model requires the consideration of the control modes and constraints imposed by such facilities. Compressor stations, for instance, are typically flow or outlet pressure controlled and have a limited operating region, which is limited by, for example, the maximum compression ratio (or adiabatic head) and the maximum available shaft power, while UGS facilities have a maximum withdrawal rate, which depends on the available working gas inventory. For each non-pipe facility we add an additional (non-linear) equation describing its control mode or active constraint. Tables 1 & 2 give an overview of different control modes and constraints for non-pipe facilities, while Table 3 lists the mathematical formulation of the control modes and constraints in Table 1.

The system of equations describing the behaviour of the total gas system can be expressed by the following matrix equation:

$$\begin{pmatrix} \Phi & -\mathbf{A} & \mathbf{I} \\ \mathbf{C_p} & \mathbf{C_Q} & \mathbf{0} \\ \mathbf{K_p} & \mathbf{K_Q} & \mathbf{K_L} \end{pmatrix} \begin{pmatrix} p^{n+1} \\ Q^{n+1} \\ L^{n+1} \end{pmatrix} = \begin{pmatrix} \Phi p^n \\ D \\ S \end{pmatrix} \tag{10}$$

where the set of equations in the first row describe the continuity equation, the second row the linearised equation for pipe and non-pipe elements (compressor stations, regulator stations, valves etc.) and the third row the control or active costraint of non-pipe facilities modelled as single nodes, such as LNG terminals, UGS and GFPPs (see Tables 1–3). The simulation grid is generated by using a dynamic time step method, where the time step Δt is set between 60–900 [s] depending on the control changes of non-pipe facilities. The space size Δx, however, remains unchanged during the time integration process and is chosen such that the ratio between the pipe length l and diameter D does not exceed 30,000 [39].

The algorithm for solving the gas model and for managing the control and constraints of non-pipe facilities is detailed in previous publications [29,38]. Moreover, the accuracy of the presented gas model has been confirmed in previous publications [15,38], where it was benchmarked against a commercial gas simulation software.

2.2. Electric power system model

Similar to a gas network, a power transmission system can be described by a directed graph $G = (V, E)$ consisting of a set of nodes V and a set of branches E, where each branch $e \in E$ represent a transmission line or a transformer and each node $i \in V$ a connection point between two or more electrical components, also referred to as bus. At some of the buses power is injected into the network by generation units, while at others power is consumed by system loads.

In contrast to gas systems, electric power systems are predominantly in steady state operation or in a state that could, with sufficient accuracy, be regarded as steady state [30]. Thus, the 3-phase transmission system is typically modelled as a balanced per phase equivalent system using linear models for the elements involved in the transport process. Fig. 2 and Table 4 give an overview of the most important elements comprising an electric power system and their mathematical representation.

Transmission lines and transformers, for instance, can be described by their branch admittance matrix derived from the generic branch model (π-circuit) depicted in Fig. 2. The elements of the branch admittance matrix can be used to compose the bus admittance matrix $\mathbf{Y_{bus}}$ for the entire network, which correlates the vector of complex bus current injections $\mathbf{I}$ to the vector of complex bus voltages $\mathbf{V}$ as follows:

[5] The convective term is negligible compared to the other terms in the momentum equation, since the flow velocity v is much smaller than the speed of sound c. A more detailed discussion is given in [38].

Table 1
Overview of available control modes and constraints settings for non-pipe facilities modelled as elements. Values in rounded brackets indicate default values for constraints.

Facility	Control Mode	Constraints
Compressor Station 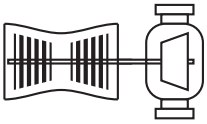	Inlet pressure ($p_{i,set}$) Outlet pressure ($p_{o,set}$) Pressure ratio (Π_{set}) Pressure difference (Δp_{set}) Flow rate (Q_{set}) Volumetric flow ($Q_{vol,set}$) Flow velocity (V_{set}) Shaft power (PWS_{set}) Driver power (PWD_{set}) Driver fuel ($Q_{f,set}$) Closed (*OFF*) Bypass (*BP*)	Internal hard limits: $p_o \geqslant p_i$ & $Q \geqslant 0$ User defined limits: max. outlet pressure ($p_{o,max}$, 80 [bar-g]) min. inlet pressure ($p_{i,min}$, 25 [bar-g]) max. volumetric flow ($Q_{vol,max}$, 100 [m^3/s]) max. flow rate (Q_{max}) max. pressure ratio (Π_{max}, 2 [–]) max. driver power (PWd_{max}, 100 [MW])
Regulator Station 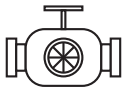	Inlet pressure ($p_{i,set}$) Outlet pressure ($p_{o,set}$) Pressure difference (Δp_{set}) Flow rate (Q_{set}) Volumetric flow ($Q_{vol,set}$) Flow velocity (V_{set}) Closed (*OFF*) Bypass (*BP*)	Internal hard limits: $p_i \geqslant p_o$ & $Q \geqslant 0$ User defined limits: max. outlet pressure ($p_{o,max}$, 80 [bar-g]) min. inlet pressure ($p_{i,min}$, 25 [bar-g]) max. volumetric flow ($Q_{vol,max}$, 100[m^3/s]) max. flow rate (Q_{max})
Valve Station 	Closed (*OFF*) Opened (*BP*)	Internal hard limit: $v \leqslant 60$ [m/s] User defined limits: max. flow velocity (v_{max}, 30 [m/s])

Table 2
Overview of available control modes and constraints settings for non-pipe facilities modelled as nodes.

Facility	Control Mode	Constraints
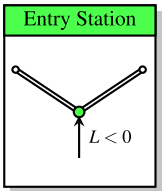	Pressure (p_{set}) Inflow (Q_{set})	Internal hard limits: $L \leqslant 0$ User defined limits: min. supply flow (Q_{min}) max. supply flow (Q_{max}) min. supply pressure (p_{min}) max. supply pressure (p_{max})
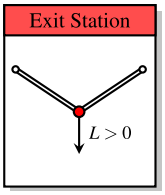	Pressure (p_{set}) Outflow (Q_{set})	Internal hard limits: $L \geqslant 0$ User defined limits: min. delivery flow (Q_{min}) max. delivery flow (Q_{max}) min. delivery pressure (p_{min}) max. delivery pressure (p_{max})
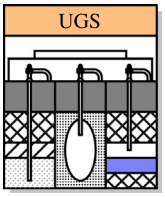	Pressure (p_{set}) Withdrawal/injection rate (Q_{set}) Initial working inventory (*INV*) Withdrawal state (*WDR*) Injection state (*INJ*)	Internal hard limits: $L^{wdr} \leqslant 0$ & $L^{inj} \geqslant 0$ User defined hard limits: max. working inventory ($I_{w,max}$) max. withdrawal rate ($Q_{wdr,max}$) max. injection rate ($Q_{inj,max}$) user defined limits: max. supply pressure ($p_{wdr,max}$) min. offtake pressure ($p_{inj,min}$)
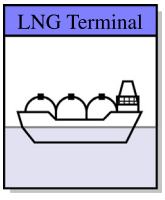	Pressure (p_{set}) Regasification rate (Q_{set}) Initial working inventory (*INV*)	Internal hard limits: $L \leqslant 0$ User defined hard limits: max. working inventory ($I_{w,max}$) max. regasification rate ($Q_{reg,max}$) user defined limits: max. supply pressure ($p_{reg,max}$)

$$\mathbf{I} = \mathbf{Y_{bus}}\mathbf{V}, \quad \mathbf{Y_{bus}} = \left[Y_{ij}\right]^{N_b \times N_b} \tag{11}$$

The steady state of an electric power system is described by the following set of non-linear algebraic equations, describing the active and reactive power balance derived from Kirschhoff's current law (KCL) and applied to each bus *i*, which basically means that all incoming and outgoing active and reactive power flows at each bus must sum up to zero.

Table 3
Control modes for non-pipe facilities and their mathematical implementation.

Control mode	Equation	Coefficients $c_1 \cdot p_1 + c_2 \cdot p_2 + c_3 \cdot Q = d$
Inlet pressure ($p_{i,set}$)	$p_i = p_{i,set}$	$c_1 = 1,\ c_2 = 0,\ c_3 = 0,\ d = p_{i,set}$
Outlet pressure ($p_{o,set}$)	$p_o = p_{o,set}$	$c_1 = 0,\ c_2 = 1,\ c_3 = 0,\ d = p_{o,set}$
Pressure ratio (Π_{set})	$\frac{p_o}{p_i} = \Pi_{set}$	$c_1 = -\Pi_{set},\ c_2 = 1, c_3 = 0,\ d = 0$
Pressure difference (Δp_{set})	$p_o - p_i = \Delta p_{set}$	$c_1 = -1,\ c_2 = 1, c_3 = 0,\ d = \Delta p_{set}$
Flow rate (Q_{set})	$Q = Q_{set}$	$c_1 = 0,\ c_2 = 0,\ c_3 = 1,\ d = Q_{set}$
Volumetric flow ($Q_{vol,set}$)	$Q = \frac{p_i}{Z_i T_i R \rho_n} Q_{vol,set}$	$c_1 = -\frac{Q_{vol,set}}{Z_i T_i R \rho_n},\ c_2 = 0, c_3 = 1,\ d = 0$
Shaft power (PWs_{set})	$PWs_{set} = \frac{K_i Q}{c_\kappa}\left[\Pi^{c_\kappa} - 1\right],\ K_i = \frac{Z_i T_i R \rho_n}{\eta_{ad}},\ \Pi = \frac{p_o}{p_i},\ c_\kappa = \frac{\kappa - 1}{\kappa}$	$c_1 = -\frac{K_i Q}{p_i}\Pi^{c_\kappa},\ c_2 = \frac{K_i Q}{p_o}\Pi^{c_\kappa}, c_3 = \frac{K_i}{c_\kappa}\left[\Pi^{c_\kappa} - 1\right],\ d = PWs_{set}$
Driver power (PWd_{set})	$PWd_{set} = \frac{K_i Q}{c_\kappa}\left[\Pi^{c_\kappa} - 1\right],\ K_i = \frac{Z_i T_i R \rho_n}{\eta_{ad}\eta_m},\ \Pi = \frac{p_o}{p_i},\ c_\kappa = \frac{\kappa - 1}{\kappa}$	$c_1 = -\frac{K_i Q}{p_i}\Pi^{c_\kappa},\ c_2 = \frac{K_i Q}{p_o}\Pi^{c_\kappa}, c_3 = \frac{K_i}{c_\kappa}\left[\Pi^{c_\kappa} - 1\right],\ d = PWd_{set}$
Driver fuel ($Q_{f,set}$)	$Q_{f,set} = \frac{K_i Q}{c_\kappa}\left[\Pi^{c_\kappa} - 1\right],\ K_i = \frac{Z_i T_i R \rho_n}{\eta_{ad}\eta_m GCV},\ \Pi = \frac{p_o}{p_i},\ c_\kappa = \frac{\kappa - 1}{\kappa}$	$c_1 = -\frac{K_i Q}{p_i}\Pi^{c_\kappa},\ c_2 = \frac{K_i Q}{p_o}\Pi^{c_\kappa}, c_3 = \frac{K_i}{c_\kappa}\left[\Pi^{c_\kappa} - 1\right],\ d = Q_{f,set}$
Bypass (*BP*)	$p_i = p_o$	$c_1 = -1,\ c_2 = 1,\ c_3 = 0,\ d = 0$
Off (*OFF*)	$Q = 0$	$c_1 = 0,\ c_2 = 0,\ c_3 = 1,\ d = 0$

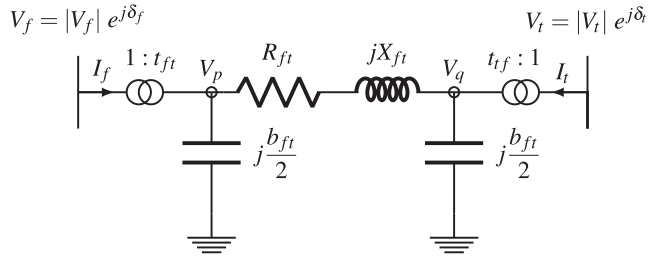

$$\begin{bmatrix} I_f \\ I_t \end{bmatrix} = \begin{bmatrix} a_{ft}^2 (y_{ft} + \frac{b_{ft}}{2}) & -t_{ft}^* \cdot t_{tf} \cdot y_{ft} \\ -t_{tf}^* \cdot t_{ft} \cdot y_{ft} & a_{tf}^2 (y_{ft} + \frac{b_{ft}}{2}) \end{bmatrix} \begin{bmatrix} V_f \\ V_t \end{bmatrix}$$

$$t_{ft} = \frac{V_p}{V_f} = a_{ft}\ e^{j\phi_{ft}},\ t_{tf} = \frac{V_t}{V_q} = a_{tf}\ e^{j\phi_{tf}},\ y_{ft} = \frac{1}{R_{ft} + jX_{ft}}$$

Fig. 2. Generic branch model (π-circuit) for modelling transmission lines ($t_{ft} = t_{tf} = 1$), in phase ($\phi_{ft} = \phi_{tf} = 0$) and phase shifting ($\phi_{ft} \neq 0 \vee \phi_{tf} \neq 0$) transformers. The characteristic of each component is expressed by its branch admittance Matrix which relates the complex current injections ($I_f,\ I_t$) at the from and to bus to the corresponding complex bus voltages ($V_f,\ V_t$).

$$G_{P,i} = P_i(\mathbf{V}) - P_{G,i} + P_{D,i} = 0, \quad i = 1 \ldots N_b \tag{12}$$

$$G_{Q,i} = Q_i(\mathbf{V}) - Q_{G,i} + Q_{D,i} = 0, \quad i = 1 \ldots N_b \tag{13}$$

$$P_i(\mathbf{V}) = \sum_{j=1}^{N_b} |V_i||V_j||Y_{ij}| \cos(\delta_i - \delta_j - \theta_{ij}) \tag{14}$$

$$Q_i(\mathbf{V}) = \sum_{j=1}^{N_b} |V_i||V_j||Y_{ij}| \sin(\delta_i - \delta_j - \theta_{ij}) \tag{15}$$

$$Y_{ij} = |Y_{ij}|(\cos(\theta_{ij}) + j \sin(\theta_{ij})) \tag{16}$$

where $P_i(\mathbf{V})$ and $Q_i(\mathbf{V})$ are the active and reactive branch flows entering or leaving bus i, respectively, $P_{G,i}$ and $Q_{G,i}$ the active and reactive power injections into bus i by power generation units, respectively, and $P_{D,i}$ and $Q_{D,i}$ the active and reactive power extractions at bus i by large industrial customers directly served from the transmission grid or by the local distribution system delivering electric power to households, businesses and small industries.

Similar to the gas system, the operation of an electric power system is restricted by a number of constraints, which if violated can lead to severe contingencies. Transmission lines, for instance, have a maximum transmission capacity S^{max}, which if exceeded can lead to outages. Generation units, in turn, can only operate within a specific operating envelope (generator capability curve), which is restricted by the upper and lower limits on active and reactive power generation P_G^{max}, P_G^{min}, Q_G^{max} and Q_G^{min}, respectively. Moreover, electric power delivered to directly served customers and local distribution systems must satisfy a contracted minimum voltage level $|V^{min}|$, to avoid legal penalties and outages in the subsystems connected to the transmission grid.

In order to operate the electric power system in an economic and secure way power TSOs are equipped with a number of simulation models to schedule the operation and control of generation units, in order to minimize total operation costs and to ensure security of supply, taking into account the changes in the electricity market and the legal and technical constraints imposed by stakeholders and power system components. The determination of an optimal generation schedule usually involves a successive solution of three different optimisation problems, namely, the unit commitment (UC), economic dispatch (ED) and reserve allocation (RA) [13,18,40]. The UC, which is described by a mixed integer linear optimisation model, determines a cost optimal schedule of when to operate which generation unit, taking into account its fixed and marginal operating costs, its ramp rate and its start-up and shut-down times and costs. The solution of the UC is used as input to the ED to compute the cost-optimal power dispatch schedule for each committed unit. The ED typically involves solving a (non-) linear constrained optimisation problem, where the objective is to find a solution for the state variables (voltage angle δ, voltage magnitude $|V|$, active and reactive power generation P_G and Q_G) that satisfies the electric power system constraints and minimizes the operational costs, which is typically expressed as a function of the active power generation $P_{G,i}$ for each committed unit i. The UC and ED are complemented by the RA, which ensures that a minimum amount of generation capacity is reserved and available to mitigate any unexpected contingency in the electric power system. The UC and ED are typically solved one day ahead of the actual operating day as well as in real-time intra-day operation, while the spinning reserves are only allocated in the day-ahead scheduling. In real-time operation the UC is normally computed every 15 [min], while the real time power dispatch is executed every 5–15 [min] [13]. Thus, the ED reflects reasonably well the operation of the electric power system, in particular, the real-time power generation dispatch. Therefore, we will use the ED to determine the changes of the state variables to the time varying electric power system loads for each simulation time step. In order to keep the complexity of the combined simulation model at a moderate level, we assume that all generation units in the model are involved in the real-time power dispatch. Thus, we omit solving the UC. However, for the transition between two consecutive simulation time steps t_{n+1} and t_n we consider key parameters that are typically included in the UC model, such as the ramp rate ω_r and the start-up T_s and shut-down T_d time for each generation unit, which we integrate into the ED model.

Table 4
Basic components in an electric network model.

Facility	Function	Constraints
Bus 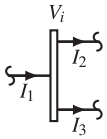	Connection point between transmission lines, transformers, generation units, loads, capacitors & reactors	Upper and lower limits on voltage magnitude $\|V_{min}\| \leqslant \|V\| \leqslant \|V_{max}\|$
Generation 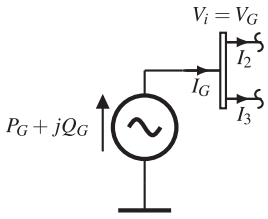	Injects electric power into the power system, by converting primary energy sources (oil, gas, coal, wind, hydro etc.) to electric energy; bus voltage V_i and frequency f_i at buses connected to generation units are typically controlled at a specific set point V_G, f_G	Upper and lower limit on reactive power Q_G and active power P_G restricted by reactive power capability curve of generation unit $P_{G,min} \leqslant P_G \leqslant P_{G,max}$ & $Q_{G,min} \leqslant Q_G \leqslant Q_{G,max}$ (i.e. operating region is restricted by field current heating limit, stator current heating limit & end region heating limit)
Load 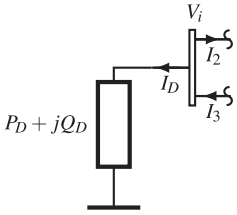	Represents consumption of electric power by large customers directly served from the transmission grid or the total power consumption from the local distribution grid connected to the transmission system at the respective substation	
Shunt Capacitor/Reactor 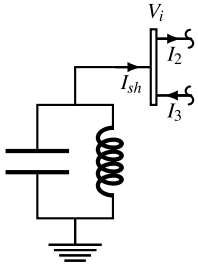	Shunt reactors are placed locally to control the steady state over-voltages at buses under light load conditions, while shunt capacitors are used to boost a bus voltage in a stressed system	

The basic ED model can be expressed by the following non-linear constraint optimisation problem:

$$\min_{\mathbf{x}} \quad f(\mathbf{P_G}) = \sum_{i=1}^{N_g} c_{0,i} + c_{1,i} P_{G,i} + c_{2,i} P_{G,i}^2 \tag{17}$$

$$s.t. \quad G_{P,i}(\mathbf{X}) = 0, \quad i = 1 \ldots N_b \tag{18}$$

$$G_{Q,i}(\mathbf{X}) = 0, \quad i = 1 \ldots N_b \tag{19}$$

$$H_k^f(\mathbf{X}) = S_k^{f^*} \cdot S_k^f - S_k^{max^2} \leqslant 0, \quad k = 1 \ldots N_l \tag{20}$$

$$H_k^t(\mathbf{X}) = S_k^{t^*} \cdot S_k^t - S_k^{max^2} \leqslant 0, \quad k = 1 \ldots N_l \tag{21}$$

$$\delta_i = \delta_i^{ref}, \quad i = i_{ref} \tag{22}$$

$$|V_i^{min}| \leqslant |V_i| \leqslant |V_i^{max}|, \quad i = 1 \ldots N_b \tag{23}$$

$$P_{G,i}^{min} \leqslant P_{G,i} \leqslant P_{G,i}^{max}, \quad i = 1 \ldots N_g \tag{24}$$

$$Q_{G,i}^{min} \leqslant Q_{G,i} \leqslant Q_{G,i}^{max}, \quad i = 1 \ldots N_g \tag{25}$$

where the decision variables expressed by vector $\mathbf{X}$

$$\mathbf{X} = [\Delta \quad \mathbf{V_m} \quad \mathbf{P_G} \quad \mathbf{Q_G}]^T \tag{26}$$

are the set of bus voltage angles Δ, bus voltage magnitudes $\mathbf{V_m}$ and active and reactive power generation at generation buses $\mathbf{P_G}$ and $\mathbf{Q_G}$, respectively. Eq. (17) is a scalar quadratic objective function, which describes the total operating costs for each generation unit in terms of its active power generation, while the non-linear equality constraints expressed by eq. (18) & (19) describe the set of active and reactive power balance Eqs. (12)–(16). Eq. (20) & (21) are non-linear inequality constraints, which describe the thermal capacity limits of each line or transformer, while the upper and lower limits of the decision variables are described by Eqs. (23)–(25). For each isolated sub network one bus is chosen as the voltage angle reference (see eq. (22)), i.e. the voltage angle of the reference bus is set to zero.

The basic ED can be solved for each simulation time step t_n to capture the behaviour of the electric power system. However, for the scope of this paper, namely, the assessment of security of supply in coupled gas and electric power systems in scenarios where both systems operate close to their limits, the basic formulation of the ED described above may not be suitable. For instance, in a contingency scenario, where total power demand exceeds total available power generation capacity, due to a disruption in a major power plant, the basic ED would not converge to a feasible solution. However, in practice in such a situation the power TSO will deploy demand side measures, like for instance, load shedding at

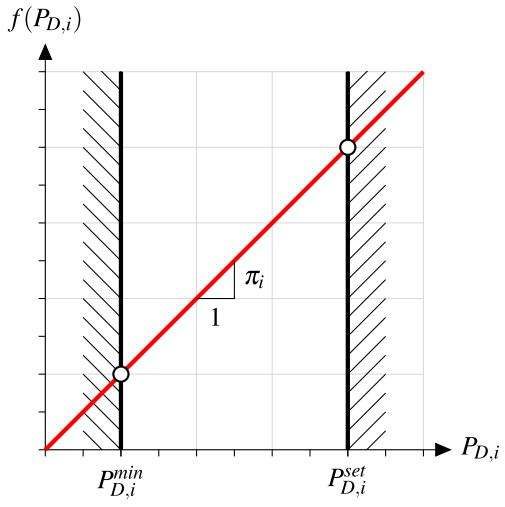

Fig. 3. Linear penalty function $f(P_{D,i})$ and constraints for dispatchable loads. The active power load can vary between the scheduled load $P_{D,i}^{set}$, which is typically given by the load profile, and the minimum load $P_{D,i}^{set}$ which is greater or equal zero. The coefficient π_i of the penalty function is the slope of the penalty curve and is referred to as the penalty factor. The penalty factor can be used to assign priority levels to the different customers connected to the power grid. The higher the penalty factor the less likely a facility will be affected by demand side measures.

specific locations based on a contingency protocol,[6] in order to maintain a secure operation of the electric power system. To account for such scenarios, we introduce the concept of dispatchable loads [41] as depicted in Fig. 3. The set of active power demand $\mathbf{P_D}$ at buses is added to the vector of decision variables $\mathbf{X}$ for the basic ED (see eq. (27)) as follows:

$$\mathbf{X} = [\Delta \quad \mathbf{V_m} \quad \mathbf{P_G} \quad \mathbf{Q_G} \quad \mathbf{P_D}]^T \tag{27}$$

In addition, the objective function in eq. (17) is extended by a linear penalty function with respect to $\mathbf{P_{D,i}}$ and the upper and lower limits on the new decision variables are added to the linear inequality constraints of the basic ED:

$$\min_{\mathbf{X}} \quad f(\mathbf{X}) = f(\mathbf{P_G}) - \sum_{i=1}^{N_b} \pi_i P_{D,i} \tag{28}$$

$$P_{D,i}^{min} \leqslant P_{D,i} \leqslant P_{D,i}^{set}, \quad i = 1 \ldots N_b \tag{29}$$

The penalty function for dispatchable loads is subtracted from the total active power generation costs $f(\mathbf{P_G})$ which are always greater than zero, thus, the solution for $P_{D,i}$ will tend to fulfil the scheduled electric power demand $P_{D,i}^{set}$ if generation and transmission capacities are sufficient to balance the power system loads and if bus voltage limits are not active. $P_{D,i}^{set}$ is set as the upper limit for the active power load $P_{D,i}$, while the lower limit $P_{D,i}^{min}$ can be set according to the contractual agreement with the customer (e.g. agreement on firm capacity and interruptible loads). As illustrated in Fig. 3 the slope of the linear penalty curve is represented by the penalty factor π_i, which we define as follows:

$$\pi_i = \xi \cdot \max_{P_{G,k}^{min} \leqslant P_{G,k} \leqslant P_{G,k}^{max}} \left\{ \left\| \frac{\partial f_k(P_{G,k})}{\partial P_{G,k}} \right\| \right\} \cdot \lambda_i, \quad k = 1 \ldots N_g, \quad 1 \leqslant \xi \leqslant 2 \tag{30}$$

where λ_i is the priority factor for the corresponding load $P_{D,i}$, which can be used to assign different priority levels to each individual customer connected to the power grid. This way, in cases where load shedding is required to balance the power system, customers with high priority factors are less likely to be affected by such demand side measures than customers with low priority factors. The priority factor is multiplied with the largest possible absolute value of the first derivative of the cost function for active power generation, in order to ensure that the solution for dispatchable loads converges to the scheduled load $P_{D,i}^{set}$ as long as power system constraints are not active (e.g. generation capacity covers scheduled loads and power losses and minimum voltage limits are not active).

The solution of the extended ED for a time step t_n is independent of the solution of a previous or future time step t_{n-1} or t_{n+1}, respectively. However, in real time power system operation there are specific transitional constraints between consecutive time steps, which restrict the operation and flexibility of the power system. In this studies, we consider the following three transitional constraints, which are key constraints in the UC model, namely, the ramp rate, the start-up time and the shut-down time, which we define similar to [42] and integrate into the extended ED model, as follows:

(1) **Ramp rate (ω_r):**
The ramp rate is the average speed in [MW/min] at which the active power generation $P_{G,i}^{n+1}$ at simulation time t_{n+1} can be increased or decreased between the minimum and maximum active power generation limit $P_{G,i}^{min}$ and $P_{G,i}^{max}$, respectively. Hence, the upper ($P_{G,i}^{max,n+1}$) and lower limit ($P_{G,i}^{min,n+1}$) on active power generation of plant i at each simulation time step t_{n+1} can be expressed as follows:

$$P_{G,i}^{max,n+1} = \min\left\{P_{G,i}^{max}; P_{G,i}^{n} + \omega_r \cdot \Delta t\right\} \tag{31}$$

$$P_{G,i}^{min,n+1} = \max\left\{P_{G,i}^{min}; P_{G,i}^{n} - \omega_r \cdot \Delta t\right\} \tag{32}$$

(2) **Start-up time (T_s):**
The start-up time is the time span between activating the power plant and the time after which the power plant reaches its minimum active power generation level $P_{G,i}^{min}$. The start-up time depends on the plant type and the time duration between the last shut-down time and the requested start-up time (i.e. cold start, warm start or hot start [42]). To account for this characteristic, we assume the following exponential function to determine the start-up time in respect to the last offline time t_o and the time t_n at which the start-up of the power plant is requested:

$$T_s(t_n, t_o) = T_s^{min} + \left(T_s^{max} - T_s^{min}\right)\left[1 - \exp\left(-5\frac{t_n - t_o}{T_o}\right)\right] \tag{33}$$

where T_s^{min} is the minimum start-up time for a hot start, T_s^{max} the maximum start-up time for a cold start and T_o is the time duration after which a station is offline and thus regarded as in cold start state. Similar to [42] we set $T_o = 72$ [h].

(3) **Shut-down time (T_d):**
We define the shut-down time as the time for the power plant to reduce its active power generation to minimum active power generation $P_{G,i}^{min}$ before finally going offline. The shut-down time depends on the ramp rate and the active power generation at the time the shut-down is requested.

The presented power system model can be solved with an interior point method, which is explained briefly in Appendix A. The

[6] Which depends on the contractual agreements with each customer, e.g. agreements on firm and interruptible loads, penalties in case of unserved electric power.

interior point method and the algorithm for solving the power system model is implemented into the simulation tool SAInt.

In the next section, we elaborate the coupling equations describing the interconnections between gas and power systems and integrate these equations into the presented gas and power system models. Moreover, we explain the algorithm for solving the resulting combined energy system.

2.3. Interdependence of gas and electric power systems

Gas and electric power systems are physically interconnected at a number of facilities. In this paper, we consider the most significant interconnections between both systems as follows:

(1) **Fuel gas demand for power generation in GFPPs connected to the gas and electric power system:**
The required fuel gas $L_{GFPP,i}$ for active power generation $P_{G,i}$ at plant i can be expressed in terms of the heat rate $HR_i(P_{G,i})$ of the GFPP and the gross calorific value GCV of the fuel gas, as follows [17]:

$$L_{GFPP,i} = \frac{HR_i(P_{G,i}) \cdot P_{G,i}}{GCV}, \quad i = 1 \ldots N_{GFPP} \tag{34}$$

The heat rate describes the amount of heat needed in [MJ] to generate and inject 1 [kW h] of electric energy into the power transmission grid. It is an indicator of the efficiency of the power plant to convert chemical energy stored in natural gas into electrical energy. It is typically expressed as a quadratic function of the active power generation $P_{G,i}$, as follows [17,43]:

$$HR_i(P_{G,i}) = \alpha_i + \beta_i \cdot P_{G,i} + \gamma_i \cdot P_{G,i}^2 \quad [\mathrm{MJ/kW\,h}] \tag{35}$$

The heat rate is the reciprocal of the thermal efficiency η_T, thus, $HR = 3.6$ [MJ/kW h] corresponds to $\eta_T = 100$ [%].

(2) **Electric power demand of EDCSs and UGS facilities:**
The electric power consumed by electric drivers can be described by the following expression[7] describing the required driver power $P_{D,i}^{CS}$ for compressing the gas flow Q from inlet pressure p_1 to outlet pressure p_2 [44]:

$$P_{D,i}^{CS} = f \frac{\kappa}{\kappa - 1} \frac{Z_1 T_1 R \rho_n Q}{\eta_{ad} \eta_m} \left[\left(\frac{p_2}{p_1} \right)^{\frac{\kappa-1}{\kappa}} - 1 \right], \quad i = 1 \ldots N_{CS} \tag{36}$$

where f is a factor describing the fraction of total driver power provided by electric drivers.

(3) **Electric power supply to LNG terminals for cooling LNG stored in tanks and for operating low and high pressure pumps required for the vaporisation process [45]:**
We capture this interaction by assuming a generic quadratic function in terms of the regasification rate L^{reg}:

$$P_{D,i}^{LNG} = k_{i,0} + k_{i,1} \cdot L_{reg,i} + k_{i,2} \cdot L_{reg,i}^2, \quad i = 1 \ldots N_{LNG} \tag{37}$$

The above coupling equations can be integrated into the gas and electric power system model by extending the external nodal load L_i in the integral continuity Eq. (1) to

$$L_i = L_{GS,i} + L_{GFPP,i} \tag{38}$$

and the active power demand $P_{D,i}$ in the active power balance Eq. (12) to

$$P_{D,i} = P_{D,i}^{PS} + P_{D,i}^{CS} + P_{D,i}^{LNG} \tag{39}$$

[7] Derived from the first and second law of thermodynamics for an isentropic compression process.

where $L_{GS,i}$ is the gas offtake or supply at non-GFPP facilities and $P_{D,i}^{PS}$ power offtake of non-gas facilities in the power grid. The resulting set of equations (10), (12), (13), (18)–(25), (28), (31)–(34), (36)–(39) describe the equilibrium state of the coupled gas and electric power system at each time step t_n. The time steps for the time integration are chosen according to the dynamic time step method for the gas model. Additional time steps are introduced if specific events in the power model occur such as the shut-down of a generation unit or outages of transmission lines.

The coupled model can be solved as a single combined system by extending the ED with additional decision variables, namely, the state variables p, Q and L and additional equality constraints expressed by the transient hydraulic gas Eqs. (3) & (5). While the computational costs for this approach may be acceptable for problems of smaller size, its application to large scale combined gas and electric power systems is connected with high computation time and storage. Thus, to speed up the solution process, we propose an iterative boundary condition adaptation method, which allows a parallel multi-threaded solution of the linearised Eqs. (3) & (A.7). The coupling equations are treated as boundary conditions, which are adapted after each iteration step k until a converged integrated solution is obtained. Moreover, we make use of the sparsity of the Jacobian matrices in eq. (3) & (5) by applying a (un-) symmetric sparse direct solver, which has been implemented into SAInt and is especially optimised for solving large sparse (un-) symmetric linear systems. We refer to [46] for more details on the sparse direct solver implemented into SAInt.

In order to start the combined dynamic gas and electric power system simulation, an initial state for the coupled system at time step t_0 is required, which can be obtained from the solution of a combined steady state simulation or from the terminal state of a combined dynamic simulation. The algorithm for solving the coupled system is described in the flow chart depicted in Fig. 4. It contains three major loops, namely, the time integration loop with the step variable t_n, the iterative loop with step variable k and the constraints and control handling (CCH) loop with step variable k_c. The CCH loop is entered, if a constraint in a gas system facility is violated (e.g. minimum pressure, maximum compression ratio violation etc.) after exiting the iterative loop. The control of the affected facility is set to the active constraint and the iterative loop is repeated.

The ramp rate for each power plant is considered by adapting the value of the upper and lower limits of the active power generation (see eq. (24)) for each simulation time step t_n such that the change in active power generation between two consecutive time steps does not exceed the ramping limits. Furthermore, we make use of the simulation control object (SCO) introduced in a previous publication [29] to control the start-up and shut down of a power plant in the course of the time integration. The SCO enables the control of a facility until a specified simulation time and/or until a specified condition is fulfilled.

The combined simulation is terminated successfully if a converged and feasible solution is obtained for each simulation time step t_n.

3. Security of energy supply parameters

The algorithm for the combined model is designed for assessing the impact of disruptions on security of energy supply in combined gas and electric power systems. In order to estimate quantitatively.

- how a disruption affected the operation of a facility or the total system,
- to compare the impact of different contingency scenarios and
- to evaluate different mitigation measures and their effectiveness,

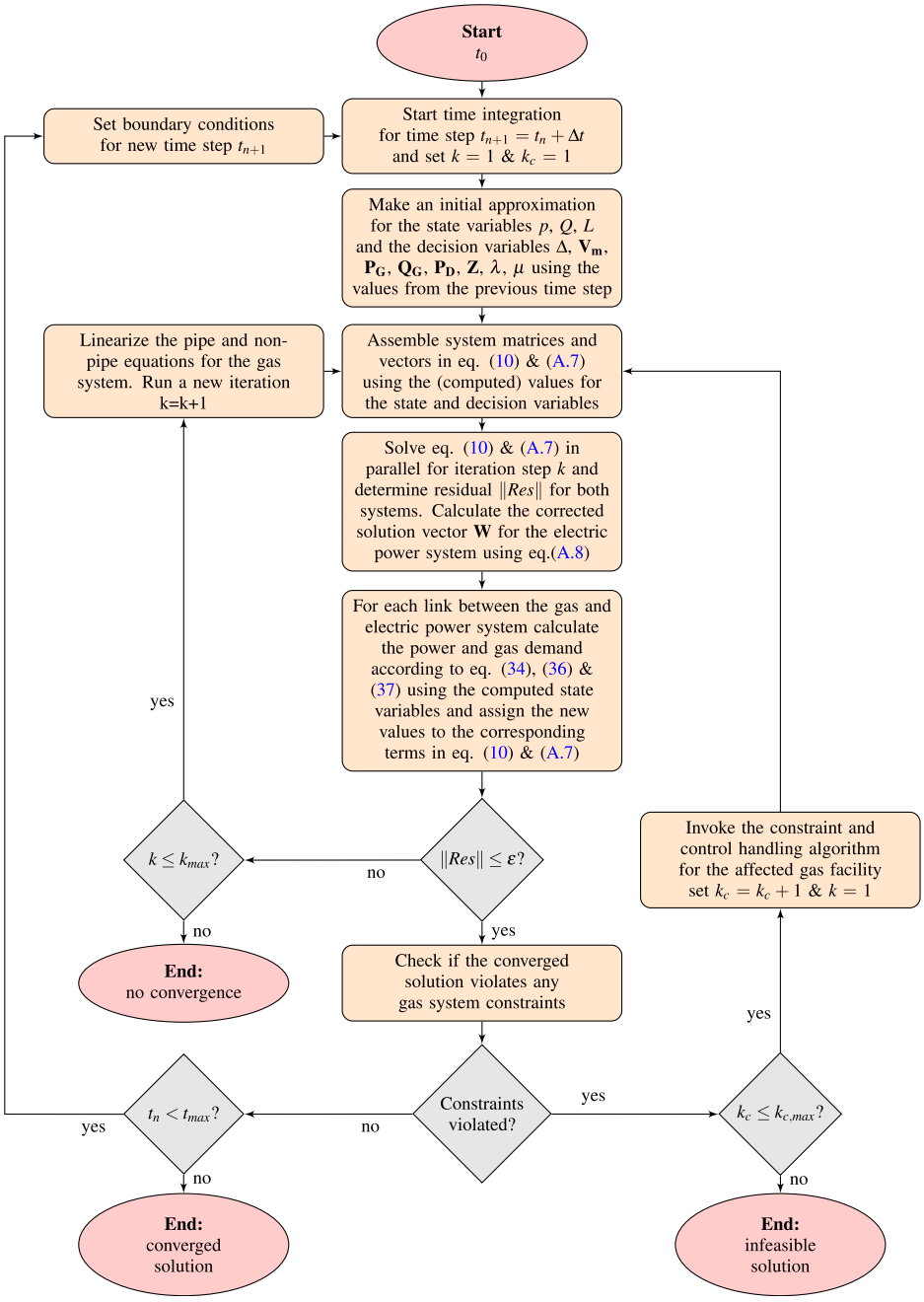

Fig. 4. Flow chart of the algorithm for solving the coupled gas and electric power system model.

we define the following parameters that serve as indicators for quantifying the impact of contingencies on security of supply:

(1) **Quantity of gas or (electric) energy not supplied (GNS/ENS):**
In case of a disruption, the quantity of gas or (electric) energy demanded by customers may not be available, due to insufficient fuel gas pressure, line pack, voltage magnitude or limited transmission capacity. The difference between the scheduled or demanded quantity of gas or (electric) energy and the actual quantity delivered to a customer (see Fig. 5) can be utilised as a quantitative indicator for the impact of a disruption on security of energy supply for a group of customers connected to the affected facility. We refer to this quantity as gas or (electric) energy not supplied (GNS/ENS), respectively. The total GNS and ENS for a gas offtake station (CGS,IND, CBE) or an electric load bus i at simulation time t_n can be determined by the following integral equations:

$$GNS_i(t_n) = \int_{t_0}^{t_n} \left[L_i^{set}(t) - L_i(t)\right] dt \tag{40}$$

$$ENS_i^g(t_n) = \int_{t_0}^{t_n} \left[L_i^{set}(t) - L_i(t)\right] \cdot GCV dt \tag{41}$$

$$ENS_i^e(t_n) = \int_{t_0}^{t_n} \left[P_{D,i}^{set}(t) - P_{D,i}(t)\right] dt \tag{42}$$

The ENS is reflected by the size of the red area depicted in Fig. 5. $L_i^{set}(t)$ and $P_{D,i}^{set}(t)$ correspond to the load profiles pre-

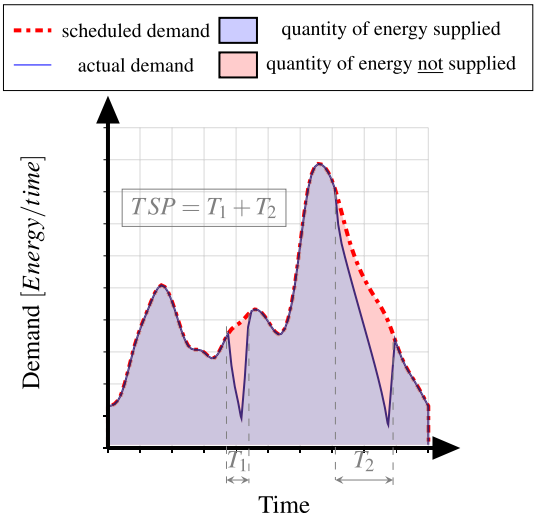

Fig. 5. Security of supply indicators.

scribed to demand nodes in the gas system (e.g. CGS, CBE, IND) and load buses in the electric power system, respectively.

(2) **Percentage of gas or (electric) energy not supplied (PENS):** The GNS and ENS of a facility gives an absolute value of the energy or gas not supplied, respectively. To evaluate the severity of the supply disruption for a facility or the total network we set the GNS/ENS in relation to the scheduled or expected energy supply and define an additional parameter referred to as percentage of scheduled energy not supplied due to a contingency, which we denote PENS. The PENS of a facility can be expressed as follows:

$$PENS_i^g(t_n) = \frac{ENS_i^g(t_n)}{\int_{t_0}^{t_n} L_i^{set}(t) \cdot GCV dt} \tag{43}$$

$$PENS_i^e(t_n) = \frac{ENS_i^e(t_n)}{\int_{t_0}^{t_n} P_{D,i}^{set}(t) dt} \tag{44}$$

The PENS can be graphically interpreted as the ratio between the red area and the sum of the red and blue area depicted in Fig. 5.

(3) **Survival time (SVT):** The indicators defined so far do not provide information on the propagation and timing of contingencies, which may be crucial for the coordination between gas and power TSOs. For instance, the time between the start time of a disruption and the time of an undesired shut down of a GFPP due to insufficient fuel gas pressure, is a good indicator of the grace period for a TSO to react and deploy counter measures to mitigate and to avoid cascading effects. Hence, a generic indicator for the resilience and the grace period to react to a contingency can be defined as the time span between the occurrence of the initial disruption t_d and the point in time at which a facility i is affected, i.e. the time t_a at which the *ENS* or *PENS* of the affected facility is greater than a predefined tolerance ϵ_{svt}. We refer to this indicator as the survival time (SVT).

(4) **Time span of energy not supplied (TSP):** The survival time indicates how long it takes until a facility is affected by a disruption, but not how long the disruption affected the facility. To account for this crucial information, we define the parameter time span of energy not supplied (TSP), which is the sum of all time intervals, where the ENS of a facility is greater zero (see Fig. 5). The TSP is an indicator of how severe a facility is affected by a contingency in terms of time.

(5) **Energy not supplied per time span (ENSTSP):** The TSP can be interpreted wrongly if a facility is affected by a disruption for a long time period, but the ENS in this time period is relatively small. To avoid this misinterpretation, we define an additional indicator for security of supply, which we refer to as energy not supplied per time span (ENSTSP), which is the ratio between ENS and TSP of a facility. The ENSTSP is the average rate of energy not supplied per time during the time intervals the facility is affected by the disruption.

The indicators presented in this section have been implemented into `SAInt` and are defined for each demand facility and for the total network system. In a previous publication [29], we implemented into `SAInt` the functionality to group the facilities in the network model into subsystems, which can then be analysed independently.[8] Thus, we can use this option to determine the value of each indicator for a specific area or group of facilities or customers, such as GFPPs and protected customers [31] (e.g. households, public services) connected to the gas or power grid. Moreover, the parameters of the subsystem can be used to declare conditional expressions for a specific action or event during the simulation. For instance, we can invoke the shut-down of a GFPP if the minimum pressure in a specific subsystem is below a certain pressure threshold or if the total ENS of the subsystem is greater zero. In the next section, we apply the developed models to a case study of a sample combined energy system.

4. Model application

The algorithm explained in Fig. 4 has been implemented into `SAInt`, a novel simulation software designed for analysing security of supply in (coupled) critical energy infrastructures. `SAInt` was developed in MS Visual Studio using the object oriented programming languages Visual Basic, Visual C#, Visual C++ and IronPython.[9] The software can be used as a standalone or combined gas and electric power system simulator. It is divided into two separate modules, namely, `SAInt-API` (Application Programming Interface) and `SAInt-GUI` (Graphical User Interface). The API is the main library of the software and contains all solvers and classes for instantiating the different objects comprising a gas and electric power system. The API is independent of the GUI and can be used separately in any other .NET environment (e.g. MS Excel, IronPython etc.).

In this section, we apply `SAInt` to perform a case study on the sample coupled gas and electric power system model depicted in Figs. 6 and 7, respectively. By doing this, we intend to demonstrate the functionality of the simulation software and capabilities of the developed model to estimate and quantify.

(1) how disruptions triggered in one system affected the operation of facilities in both systems,
(2) how disruptions propagate from one system to the other,
(3) the grace period for gas and power TSOs to coordinate and react to contingencies, and

[8] Subsystems in `SAInt` are referred to as GSUB for gas subsystems and ESUB for subsystems of the electric network.

[9] SAInt is mainly programmed with Visual Basic, however, to make use of different available open source libraries parts of the source code are written in other .NET languages, such as Visual C# and Visual C++. IronPython is used as a scripting language for interacting with the user through the command window and model tables available in the GUI. All conditional expressions for enforcing a defined boundary condition in the scenario definition tables are evaluated with the IronPython interpreter.

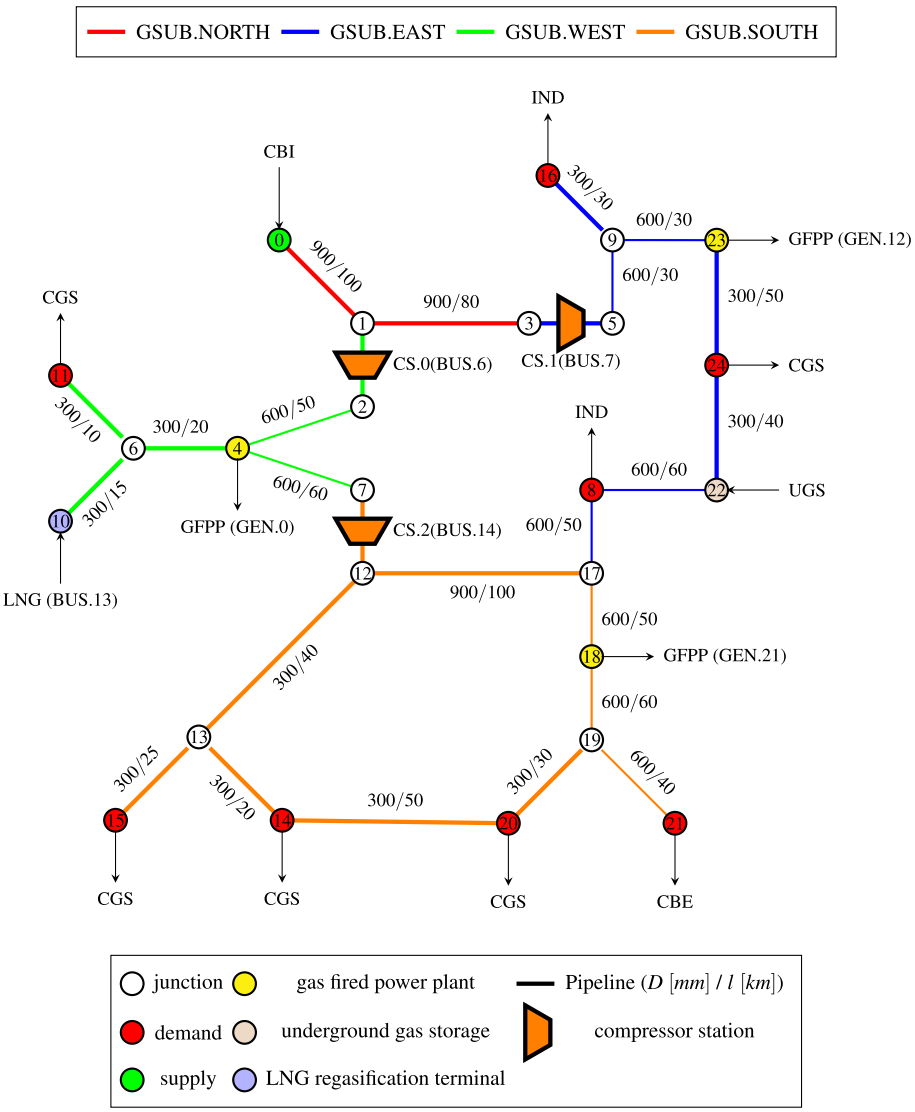

Fig. 6. 25-Node gas model used for the case studies.

(4) how effective are specific counter measures to mitigate the impact of disruptions.

Due to the scope of this study, the model cannot capture how a disruption may affect the gas or electricity market or how market based measures may help mitigate the impact of contingencies.

The gas and electric network used in the case study are bidirectionally coupled through three GFPPs (NO.4 <-> GEN.12, NO.18 <-> GEN.21, NO.23 <-> GEN.0), three EDCSs (CS.0 <-> BUS.6, CS.1 <-> BUS.7, CS.2 <-> BUS.14) and one LNG terminal (NO.10 <-> BUS.13). Two of the GFPPs (NO.18 <-> BUS.21 & NO.23 <-> BUS.0) use combined cycle gas turbines (CCGTs), while the third GFPP (NO.4 <-> GEN.12) uses conventional gas turbines (GTs) to generate electricity. The third GFPP serves as a reserve and backup for intermittent wind power generation at generation bus GEN.22, thus, the GFPP is offline unless the electric power generated by the wind turbines is below a certain threshold. The input data for the nodes, pipes, compressor stations and the LNG terminal in the gas network are given in Tables B.8–B.11, while the data for the buses, transmission lines and generators in the electric network are listed in Tables B.12–B.14. The simulation properties for the case study are given in Table 5.[10] The simulation time window for all studied scenarios is set to $T_{max} = 24$ [h] (one operating day, from 6:00 AM to 6:00 AM) for the sake of keeping the result data and discussion at a moderate size. However, the time window can be extended as desired in order to study long-term contingency scenarios. The reference time step is set to $\Delta t = 15$ [min], however, the time resolution may be adapted by the dynamic time step adaptation (DTA) method in case of control changes or changes in active constraints during the time integration process. The DTA is explained in detail in a previous publication [29].

In order to run a combined quasi-dynamic simulation, an initial state of the combined network is required, which can either be the solution of a combined steady state or the terminal state of a combined quasi-dynamic simulation. For the case study, we compute initially a combined steady state scenario and use the solution as an initial state for the combined quasi-dynamic scenarios studied in this paper. The results of the combined steady state simulation

[10] All data used for the gas and power network are available as native `SAInt` input files in the electronic version of this paper and are described further in Appendix D.1. The properties of the power plants (see Table B.14), were chosen according to the data provided by [42,47].

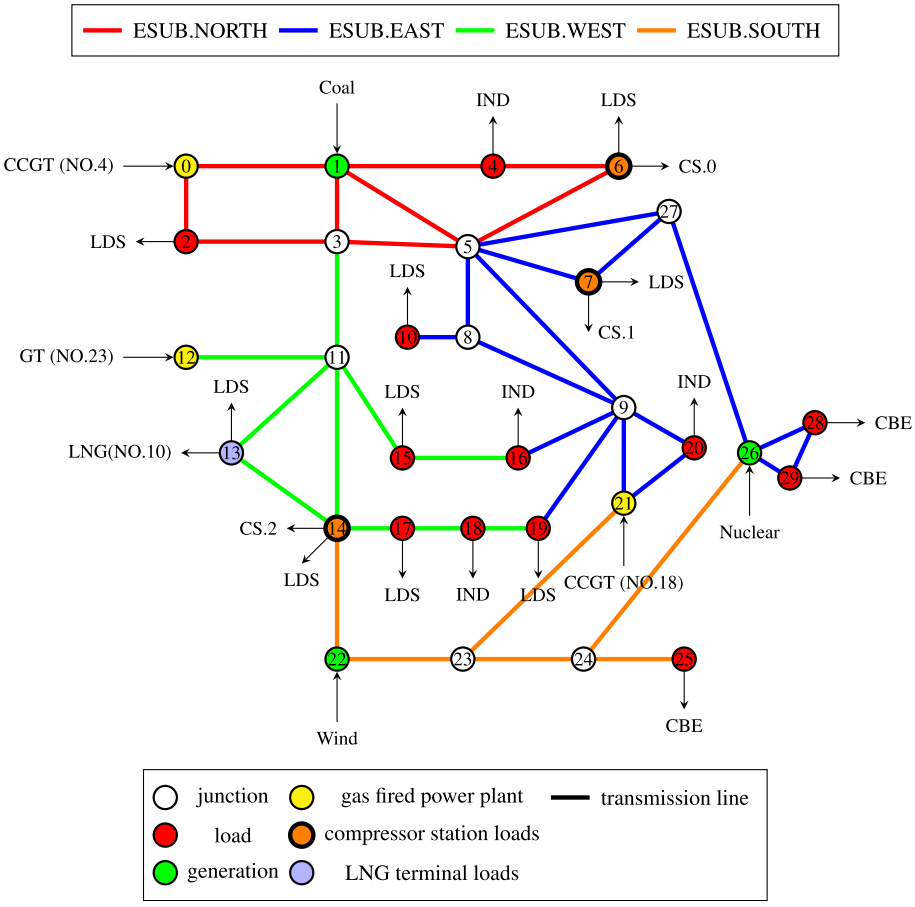

Fig. 7. Modified version of IEEE 30-Bus power system model.

Table 5
Input parameter for the sample combined gas and power transmission network.

Parameter	Symbol	Value	Unit
Reference time step	Δt	900	[s]
Total simulation time	T_{max}	24	[h]
Gas temperature	T_g	288.15	[K]
Dynamic viscosity[a]	η	$1.1 \cdot 10^{-5}$	[kg/m s]
Isentropic coefficient	κ	1.3	[–]
Reference pressure	p_n	1.01325	[bar]
Reference temperature	T_n	273.15	[K]
Critical pressure[b]	p_{crit}	45	[bar]
Critical temperature	T_{crit}	193.7	[K]
Relative density	d	0.6	[–]
Gross calorific value	GCV	41.215	[MJ/sm^3]
Nominal power	BaseMVA	100	[MVA]

[a] The dynamic viscosity of the gas is needed for calculating the Reynolds number, which, in turn is needed for computing the friction factor λ using Hofer's equation as described in [38].

[b] The critical pressure and temperature of the gas is needed for calculating the compressibility factor based on the equation developed by Papay as described in [38].

are plotted in Fig. 8 and listed in Tables C.15–C.18. The simulation protocol, which includes information of the residual for the gas model, power model and coupling equations for each step of the sequential linearisation is attached to the electronic version of this paper (SAInt-Log-SteadyState).

In the following sections, we simulate three scenarios and discuss their results. All three scenarios were computed on an Intel Core i7-3630QM 2.4 GHz CPU with 8 GB RAM and a 64-Bit Windows 10 Operating System.

4.1. Case 0 – Base case scenario with intermittent wind power generation and backup by spinning reserve GFPP

In case 0, we study a base case scenario, where wind power generation at bus GEN.22 is not available for some time intervals, due to insufficient wind velocity. We use the functionality to define conditional scenario parameters in `SAInt` to enforce the start-up of the backup GFPP connected to bus GEN.12 in case wind power generation at bus GEN.22 falls below 1 [MW] within two consecutive simulation time steps (see Fig. 4). However, the start-up of the backup GFPP, is only possible if there is enough linepack in subsystem GSUB.EAST and if the pressure in the corresponding fuel gas node (NO.23) is above 35 [bar-g], in order to avoid a minimum pressure violation at start-up ($p^{min} = 30$ [bar-g]). For all CGSs in the gas network, we assign the relative load profile depicted in the left plot of Fig. 9 and scale the value with the computed steady state loads. For all active and reactive loads at substations connected to the local distribution system (LDC) we factor the relative load profile depicted in the right plot of Fig. 9 with the steady state power system loads. All other loads in both networks are assumed constant (i.e. loads of IND & CBE). The relative profile for wind generation visualised in Fig. 10 is assigned to the wind power generator connected to bus GEN.22 and is scaled with the steady state active wind power generation (60 [MW]). Fig. 11 shows a snapshot of the `SAInt` – electric network scenario table, where the boundary conditions and the implementation of the start-up and shut down of GFPPs is illustrated.

For the given settings in case 0, we do not expect any significant impact on security of supply for both networks, since the available generation capacity provided by the backup GFPP should be

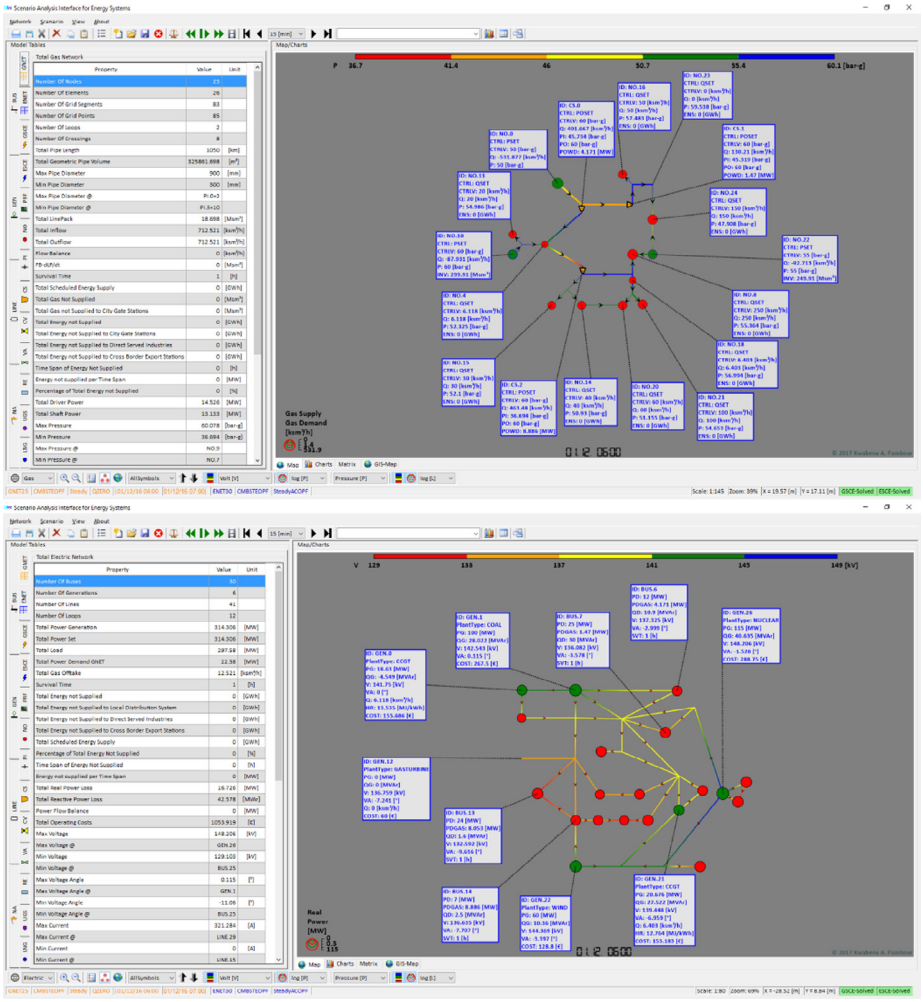

Fig. 8. Snapshot of *SAInt-GUI* showing results of the combined steady state computation for the gas (top) and electric network (bottom) applied in the case study. Diameter of the circles representing demand (red) and supply (green) nodes in the top plot correspond to the magnitude of the steady state loads in logarithmic scale, as can be seen from the legend in the bottom left corner. Colours of the pipe elements correspond to the pressure levels as indicated by the top colour bar. Pipe arrows indicate gas flow direction. Diameter of the circles representing load (red) and generation (green) buses in the bottom plot correspond to the magnitude of active power in logarithmic scale, as can be seen from the legend in the bottom left corner. Colours of the line elements correspond to the voltage levels as indicated by the top colour bar. Line arrows indicate flow direction of electric current. Labels describe the results and properties for selected objects in the combined system. (For interpretation of the references to colour in this figure legend, the reader is referred to the web version of this article.)

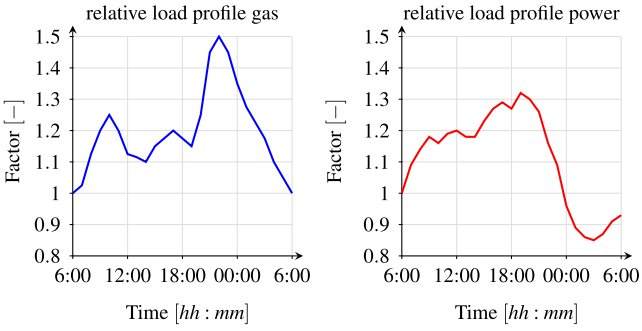

Fig. 9. Load profile assigned to CGS in gas network (left side) and active power load at buses in electric power network (right side).

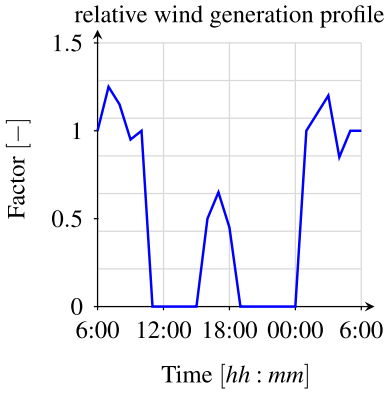

Fig. 10. Relative profile for variable and intermittent wind power generation assigned to bus GEN.22.

sufficient to cover the system loads at times of missing wind power generation.

The results for case 0 are illustrated in the time plots depicted in Figs. 12 & 15 and in the animation video SAInt_Case0 generated with *SAInt* and attached to the electronic version of this paper. The simulation protocol for case 0 SAInt-Log-Case0, which contains information on the residual for each simulation time step and the changes in control and active constraints of active gas facilities, is also available in the electronic version of the paper. The computation for case 0 took approximately 10 [sec] for 96 time steps.

SAInt - Table for ESCE

Active	Time	Object	Nr	Condition	Evaluation	Name	Parameter	Profile	Value	Unit
☑	01/12 06:00	BUS	15		NONE	Bus015	PD	LOADPRF	9	[MW]
☑	01/12 06:00	BUS	16		NONE	Bus016	PD	CONST	15	[MW]
☑	01/12 06:00	BUS	17		NONE	Bus017	QD	LOADPRF	.9	[MVAr]
☑	01/12 06:00	BUS	14		NONE	Bus014	PD	LOADPRF	7	[MW]
☑	01/12 06:00	BUS	29		NONE	Bus029	PD	CONST	35	[MW]
☑	01/12 06:00	BUS	15		NONE	Bus015	QD	LOADPRF	1.8	[MVAr]
☑	01/12 06:00	BUS	17		NONE	Bus017	PD	LOADPRF	10	[MW]
☑	01/12 06:00	BUS	20		NONE	Bus020	PD	CONST	16	[MW]
☑	01/12 06:00	BUS	25		NONE	Bus025	PD	CONST	30	[MW]
☑	01/12 06:00	BUS	28		NONE	Bus028	PD	CONST	30	[MW]
☑	01/12 06:00	BUS	18		NONE	Bus018	PD	CONST	8	[MW]
☑	01/12 06:00	BUS	19		NONE	Bus019	QD	LOADPRF	.7	[MVAr]
☑	01/12 06:00	BUS	19		NONE	Bus019	PD	LOADPRF	25	[MW]
☑	01/12 06:00	BUS	13		NONE	Bus013	QD	LOADPRF	1.6	[MVAr]
☑	01/12 06:00	BUS	6		NONE	Bus006	QD	LOADPRF	10.9	[MVAr]
☑	01/12 06:00	BUS	6		NONE	Bus006	PD	LOADPRF	12	[MW]
☑	01/12 06:00	BUS	7		NONE	Bus007	QD	LOADPRF	30	[MVAr]
☑	01/12 06:00	BUS	14		NONE	Bus014	QD	LOADPRF	2.5	[MVAr]
☑	01/12 06:00	BUS	2		NONE	Bus002	QD	LOADPRF	1.2	[MVAr]
☑	01/12 06:00	BUS	2		NONE	Bus002	PD	LOADPRF	5	[MW]
☑	01/12 06:00	BUS	10		NONE	Bus010	PD	LOADPRF	24	[MW]
☑	01/12 06:00	BUS	13		NONE	Bus013	PD	LOADPRF	24	[MW]
☑	01/12 06:00	BUS	7		NONE	Bus007	PD	LOADPRF	25	[MW]
☑	01/12 06:00	BUS	10		NONE	Bus010	QD	LOADPRF	1.75	[MVAr]
☑	01/12 06:00	GEN	22		NONE	Bus022	PG	WINDPRF	60	[MW]
☑	01/12 06:00	GEN	0	NO.4.P[barg] > 35 and GSUB.WEST.LP.[Msm3] > 1.5	DoIfTrue	Bus000	ON	-		
☑	01/12 06:00	GEN	0	NO.4.P[barg] < 30 or GSUB.WEST.LP[Msm3] < 1.5	DoIfTrue	Bus000	OFF	-		
☑	01/12 06:00	GEN	12	(GEN.22.PG.[MW] < 1 and GEN.22.PG.(time-dt).[MW] < 1) and (NO.23.P[barg] > 35 and GSUB.EAST.LP[Msm3]>5)	DoIfTrue	Bus012	ON	-		
☑	01/12 06:00	GEN	12	(GEN.22.PG.[MW] > 1 and GEN.22.PG.(time-dt).[MW] > 1) or GSUB.EAST.LP.[Msm3] < 3	DoIfTrue	Bus012	OFF	-		
☑	01/12 06:00	GEN	21	NO.18.P[barg] > 35 and GSUB.SOUTH.LP.[Msm3] > 6	DoIfTrue	Bus021	ON	-		
☑	01/12 06:00	GEN	21	NO.18.P[barg] < 30 or GSUB.SOUTH.LP.[Msm3] < 6	DoIfTrue	Bus021	OFF	-		

Fig. 11. *SAInt* scenario definition table showing the defined boundary conditions for the electric network for case 0 and the conditional expression for the shut-down and, start-up of GFPPs in respect to their corresponding nodal gas pressure and linepack in the corresponding subsystem. Each boundary condition is composed of a simulation time (i.e. time at which the boundary condition is evaluated by the solver for the first time), a reference object, a parameter and its value (the value can also be an IronPython expression referring to properties of objects in the model) and a conditional expression and its evaluation type (choice of how often the condition should be evaluated by the solver in the course of the simulation). For some parameters a profile can be assigned by specifying the profile name, after the profile is created in the *SAInt* – profile editor introduced in [29]. The variable "time" in the conditional IronPython expression denotes the elapsed simulation time in hours at which the expression is evaluated, while the variable "dt" denotes the time duration in hours between the last two consecutive simulation time steps, i.e. $dt = t_n - t_{n-1}$.

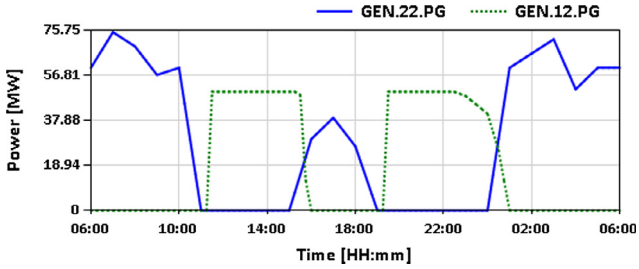

Fig. 12. Case 0 – Time plot for active power generation (*PG*) at buses GEN.12 and GEN.22.

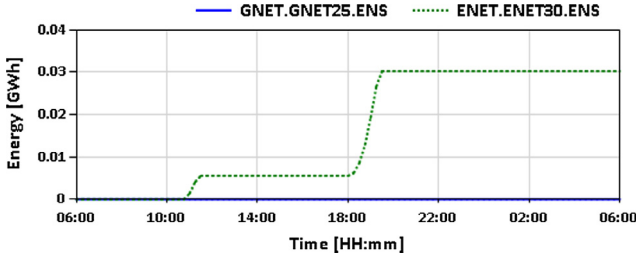

Fig. 13. Case 0 – Time plot for Energy Not Supplied (ENS) for the total gas (blue curve) and total electric network (green curve). (For interpretation of the references to colour in this figure legend, the reader is referred to the web version of this article.)

Fig. 12 shows the time evolution of the active power generation (P_G) at buses GEN.22 (blue curve, wind generation) and GEN.12 (green curve, backup GFPP). As can be seen, the GFPP starts-up whenever wind power generation is zero and shuts down whenever it is above zero. The start-up of the GFPP, however, is always delayed by approx. 30 [min] after loss of wind power generation,

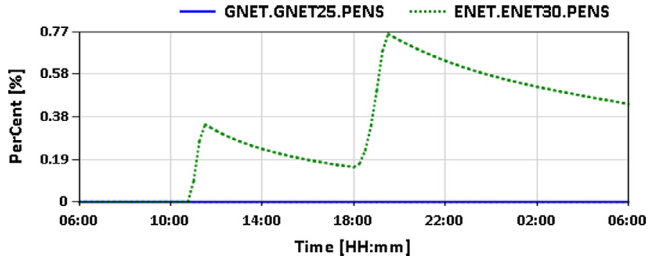

Fig. 14. Case 0 – Time plot for Percentage of Energy Not Supplied (ENS) for the total gas (blue curve) and total electric network (green curve). (For interpretation of the references to colour in this figure legend, the reader is referred to the web version of this article.)

due to the transitional constraints (limit for start-up time is $\geqslant$15 [min] for GFPPs, see Table B.14) explained in Section 2.2 and defined in Table B.14 and the conditional expression for starting-up and shutting down GFPPs after the active power generation is below or above 1 [MW] for two consecutive time steps, respectively. The impact of the delay in backup power on security of energy supply is visible in the time plot for ENS and PENS for the total gas and total electric power system depicted in Figs. 13 & 14. While the ENS and PENS for the gas system remain zero, security of supply in the electric power system is affected exactly at times, where there is a delay in backup power generation by the backup GFPP connected to GEN.12. The power system implements load shedding in order to balance the reduced generation capacity, which is visible by the increase in ENS and PENS at approx. 10:45 and 18:15. However, the impact of the load shedding is relatively small, since the PENS is less than 1 [%]. One way to avoid load shedding would be to set the wind power generation threshold for starting-up the GFPP to a higher value. However, this may also result in an increased number of start-up and shut down cycles, which, in turn, is connected to higher operational costs.

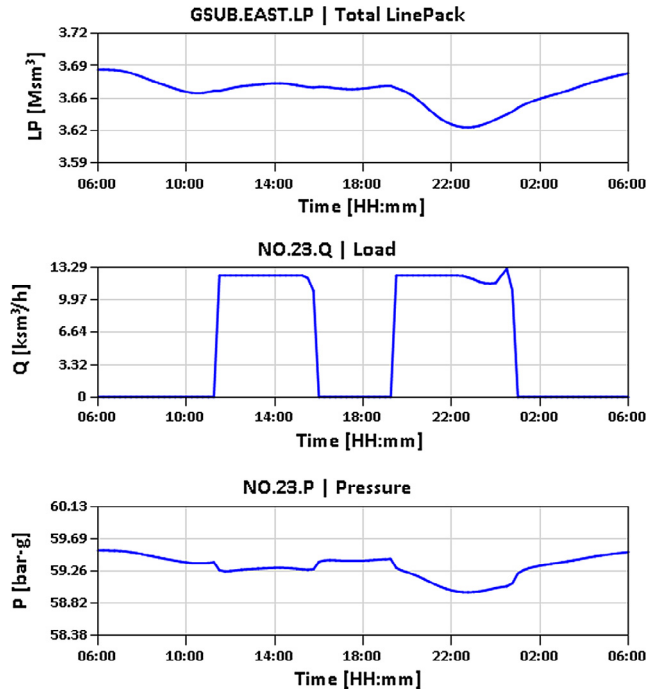

Fig. 15. Case 0 – Time plot for linepack in subsystem GSUB.EAST (*LP*), nodal pressure (*P*) and fuel gas offtake for power generation (*Q*) at node NO.4.

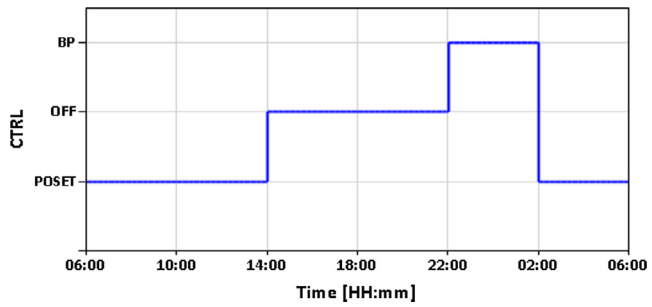

Fig. 16. Case 1 – Time plot of the station control (*CTRL*) of compressor station CS.1.

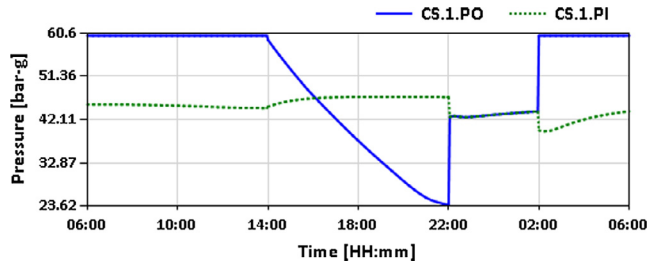

Fig. 17. Case 1 – Time plot of the inlet and outlet pressure of compressor station CS.1.

Besides, without the extension of the basic ED by the dispatchable load model derived in Section 2.2, the combined model would not have converged to a feasible solution, due to insufficient generation capacity to balance the power system loads. The ramping of the backup GFPP is possible, because there is enough pressure at the corresponding fuel gas offtake node in the gas system and sufficient linepack in the corresponding subsystem GSUB.EAST, as can be seen in Fig. 15, where the time plot of the unit state at GEN.12, the fuel gas offtake and pressure at gas node NO.23 and the linepack in subsystem GSUB.EAST is illustrated.

4.2. Case 1 – Disruption in compressor station CS.1

In this section, we examine how a disruption in compressor station CS.1 affects security of supply in the combined system. The gas flow through CS.1 is interrupted completely (OFF) at 14:00 for 8 [h], due to a failure in the compressor station.[11] At 22:00, the failure in the station is remedied, but the start-up of the station is delayed for another 4 [h]. However, in this time the flow can bypass (BP) the station without gas compression until the station returns to its original control set point at 02:00 (outlet pressure control of 60 [bar-g]). The described events are visualised in Fig. 16, where the time evolution of the control of compressor station CS.1 is depicted. All boundary conditions and settings from case 0 are carried over to case 1.

We expect a stronger impact of the disruption on security of supply in the gas network than in the electricity network. For the gas network, the disruption in CS.1 may cause the pressure and line pack in the downstream hydraulic area to drop, therefore, the scheduled gas demand in the area may not be covered due to insufficient gas pressure. This in turn, may also influence the start-up of the backup GFPP for balancing the missing wind power generation, which requires a specific fuel gas pressure and available linepack to operate.

The results for case 1 are illustrated in the time plots depicted in Figs. 16 & 23 and in the animation video SAInt_Case1 attached to the electronic version of this paper. The simulation protocol for case 1 (SAInt-Log-Case1 is also available in the electronic version of the paper. The computation for case 1 took approximately 22 [sec] for 100 time steps.

Fig. 17 shows the reaction of the inlet and outlet pressure to the disruption and the control changes at compressor station CS.1. The interruption of gas flow through the station at 14:00 caused a rapid decrease in outlet pressure and a slight increase in inlet pressure. The inlet pressure stabilizes to a constant pressure due to the pressure control at the CBI station connected to node NO.0. As can be seen in the animation video for case 1 (SAInt_Case1), the gas supply from NO.0 decreases right after the interruption of gas flow at CS.1 to avoid an overpressure in the subsystem GSUB.NORTH. The reduction of the outlet pressure is a result of an imbalance between gas offtake (IND at NO.16 & CGS at NO.24) and gas supply (UGS at NO.22) to the downstream hydraulic area (area in GSUB.EAST separated by the outlet node of CS.1 and the pressure controlled UGS node NO.22), thus, the linepack and the average pressure in the hydraulic area decreases rapidly (the flow imbalance between NO.16, NO.24 and NO.22 right after the disruption can be seen in the animation video for case 1 SAInt_Case1). The pressure and linepack in the hydraulic area decreases to an extend that at a certain simulation time the gas offtake at NO.16 and NO.24 are curtailed in order to maintain the minimum operating pressure of 25 [bar-g] and 16 [bar-g], respectively (see simulation protocol SAInt-Log-Case1 and animation video SAInt_Case1 for more details). The simulation time at which the curtailment of gas demand is initiated is shown in the time plot of the TSP for the gas network depicted in Fig. 21 (blue curve). The TSP starts increasing linearly at approx. 20:00, 6 [h] after the disruption in CS.1. This is the grace period for the gas TSO to react to the contingency, by deploying an emergency plan to mitigate or avoid the impact of the disruption on security of supply. A counter measure could be, for instance, to set the withdrawal from the UGS facility connected to node

[11] Case 1 is a hypothetical scenario to demonstrate the capability of the developed model to simulate and estimate the impact of supply disruptions. In practice, a failure in a compressor station would not necessarily result in a complete shut-down and stop of flow, but rather the flow will bypass the station without compression through a designated bypass valve system. However, in this case study, we assume the bypass valve cannot be opened, due to a technical failure.

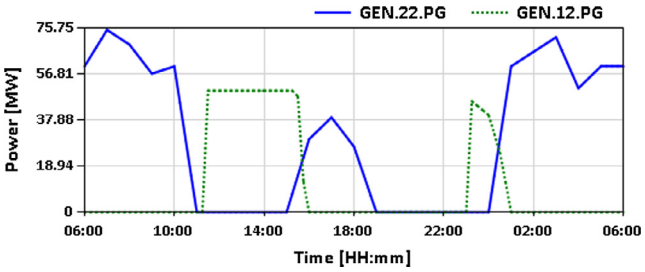

Fig. 18. Case 1 – Time plot for active power generation (*PG*) at buses GEN.12 and GEN.22.

NO.23 to maximum withdrawal capacity. The information obtained for the grace period would not be available if instead of a dynamic model a steady state gas model was used, since the imbalance between supply and demand, thus, the change in pressure and linepack cannot be reflected with the steady state approach.

The disruption in the gas system propagates also to the electric power system and affects security of supply in the power system, as can be seen in Figs. 18 & 23, where the active power generation at buses GEN.22 and GEN.12, the linepack in subsystem GSUB.EAST and the fuel gas offtake and pressure at node NO.23 are depicted. The start-up of the backup GFPP connected to bus GEN.12 after the loss of wind power generation at approximately 19:00 is delayed for a approximately 4 [h] (compare Fig. 12-12), due to insufficient fuel gas pressure at node NO.23 and linepack in subsystem GSUB.EAST. Because of this delay, the generation capacity in the electricity system is insufficient to balance the power system loads, thus, some loads in the power system are curtailed in respect to the priority factors assigned to the different load buses in Table B.12.

The impact of the disruption on security of supply for the total gas and electricity network is depicted in Figs. 19–22. In absolute terms, the gas system is more affected by the disruption than the electricity system (see Fig. 19), since the ENS for the gas network is significantly higher than the ENS for the electricity network (ca. 2 [GW h] compared to ca 0.1 [GW h]), while in relative terms, the impact is slightly higher for the electricity network than for the gas network as can be seen in Fig. 20. Furthermore, the survival time for the total gas system is 6 [h] and for the electricity system 8 [h] (see Fig. 20), assuming a survival time tolerance of $\epsilon_{svt} = 1$ [%] for the PENS of the total system. This means, the time span between the disruption event and the point in time at which the total ENS is about to exceed 1 [%] of the expected or scheduled total energy supply is 6 [h] or 8 [h], respectively. This crucial time information can be regarded as the grace period for gas and power TSOs to coordinate and react to the contingency.

Figs. 21 & 22 show how long the disruption affected the total gas and electricity system (TSP) and the average rate of energy not supplied per time span (ENSTSP). As can be seen, the power system was affected by the disruption for a longer time period than the gas system (6.3 [h] compared to 3.75 [h]). However, due to the relatively large magnitude of the ENS for the gas system compared to that for the electric power system (see Fig. 19) the ENSTSP for the gas system is significantly greater than the one for the power system.

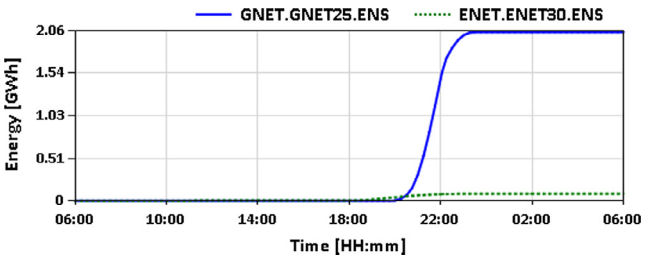

Fig. 19. Case 1 – Time plot for Energy Not Supplied (ENS) for the total gas (blue curve) and total electric network (green curve). (For interpretation of the references to colour in this figure legend, the reader is referred to the web version of this article.)

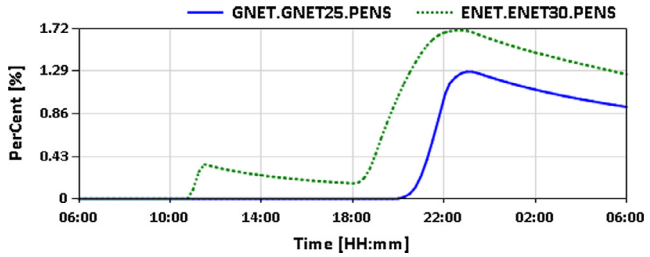

Fig. 20. Case 1 – Time plot for Percentage of Energy Not Supplied (PENS) for the total gas (blue curve) and total electric network (green curve). (For interpretation of the references to colour in this figure legend, the reader is referred to the web version of this article.)

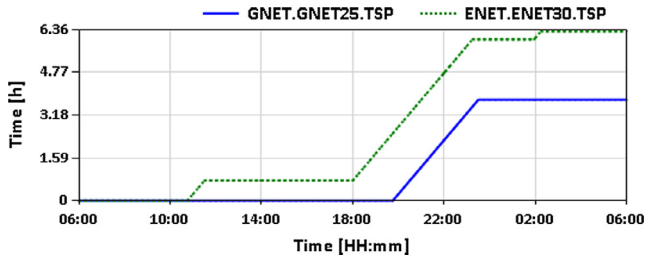

Fig. 21. Case 1 – Time plot for Time Span of Energy Not Supplied (TSP) for the total gas (blue curve) and total electric network (green curve). (For interpretation of the references to colour in this figure legend, the reader is referred to the web version of this article.)

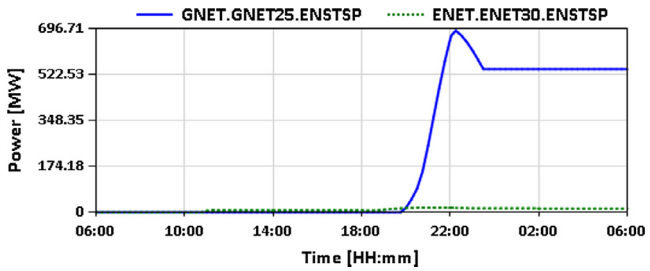

Fig. 22. Case 1 – Time plot for Energy Not Supplied per Time Span of Energy Not Supplied (ENSTSP) for the total gas (blue curve) and total electric network (green curve). (For interpretation of the references to colour in this figure legend, the reader is referred to the web version of this article.)

4.3. Case 2 – Full withdrawal capacity at gas storage facility to mitigate the impact of compressor station disruption

In this section, we investigate the effectiveness of a countermeasure to mitigate the impact of the disruption in compressor station CS.1, by enforcing the UGS facility connected to node NO.23 to increase its pressure set point to maximum operating pipeline pressure of 60 [bar-g], if the linepack in subsystem GSUB.EAST is below 3.3 [Msm^3]. All boundary conditions and events defined in case 1 a carried over to case 2.

We expect this countermeasure to reduce the impact on security of supply in the gas and electricity system. However, we expect the gas system to benefit more from the countermeasure than the

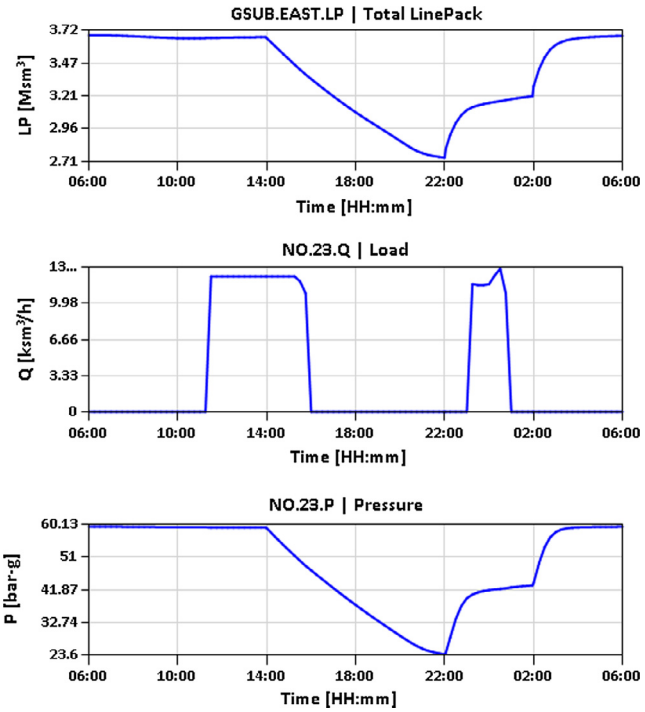

Fig. 23. Case 1 – Time plot for linepack in subsystem GSUB.EAST (*LP*), nodal pressure (*P*) and fuel gas offtake for power generation (*Q*) at node NO.4.

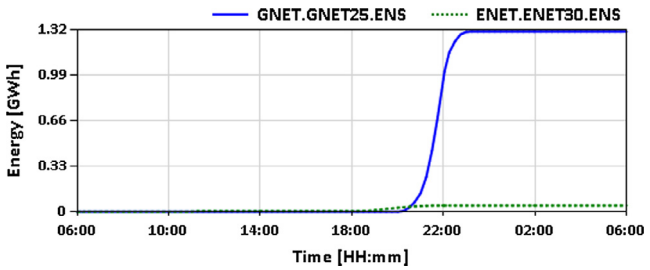

Fig. 25. Case 2 – Time plot for Energy Not Supplied (ENS) for the total gas (blue curve) and total electric network (green curve). (For interpretation of the references to colour in this figure legend, the reader is referred to the web version of this article.)

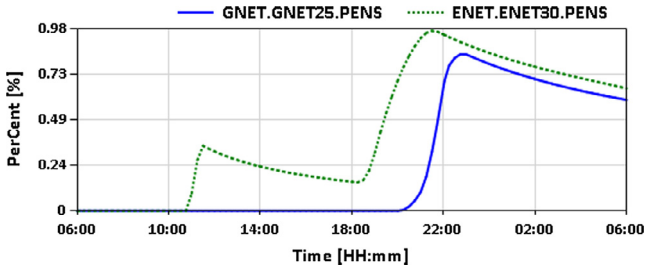

Fig. 26. Case 2 – Time plot for Percentage of Energy Not Supplied (PENS) for the total gas (blue curve) and total electric network (green curve). (For interpretation of the references to colour in this figure legend, the reader is referred to the web version of this article.)

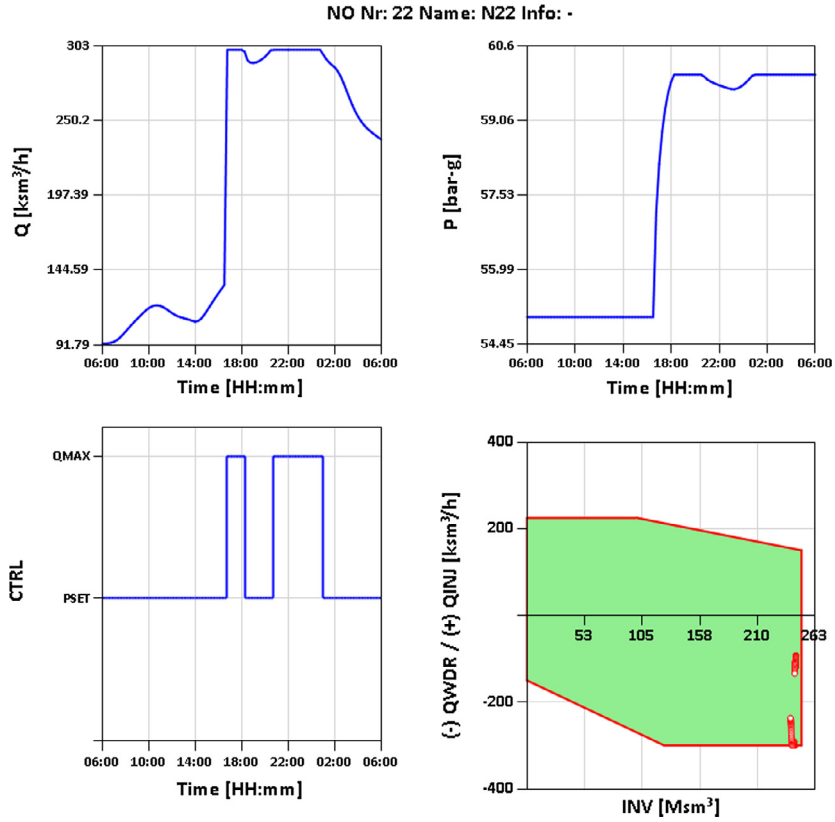

Fig. 24. Case 2 – Time plot of gas offtake (*Q*) gas pressure (*P*) station control (*CTRL*) and the operating gas storage envelope (withdrawal and injection rate versus working inventory) for the UGS facility connected to node NO.4.

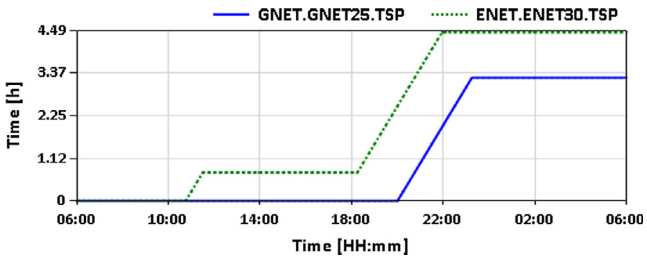

Fig. 27. Case 2 – Time plot for Time Span of Energy Not Supplied (TSP) for the total gas (blue curve) and total electric network (green curve). (For interpretation of the references to colour in this figure legend, the reader is referred to the web version of this article.)

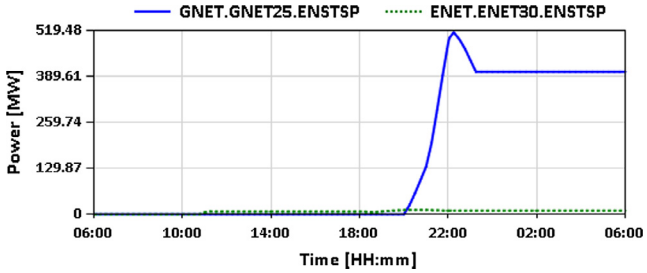

Fig. 28. Case 2 – Time plot for Energy Not Supplied per Time Span of Energy Not Supplied (ENSTSP) for the total gas (blue curve) and total electric network (green curve). (For interpretation of the references to colour in this figure legend, the reader is referred to the web version of this article.)

electricity system, since the countermeasure is applied in the gas system.

The results for case 2 are illustrated in the time plots depicted in Figs. 24 & 28 and in the animation video SAInt_Case2 attached to the electronic version of this paper. The simulation protocol for case 2 (SAInt-Log-Case2 is also available in the electronic version of the paper. The computation for case 2 took approximately 23 [sec] for 101 time steps.

Fig. 24 shows the time plot of gas offtake (Q) gas pressure (P) station control ($CTRL$) and the storage envelope showing the working points for the UGS facility connected to node NO.4. As can be seen, the UGS facility reacts to the disruption at approximately 16:45 when the linepack in subsystem GSUB.EAST is lower than 3.3 [Msm^3]. The pressure set point is increased to 60 [bar-g], however, this set point cannot be maintained at all time, due to the maximum withdrawal capacity limit of 300 [ksm^3/h] illustrated in the operating envelope of the UGS facility. The increased withdrawal from storage has a positive effect on security of supply in the gas and electricity network, which is visible, if we compare the time plots from case 1 for ENS, PENS, TSP and ENSTSP (s. Figs. 19–22) to the time plots for case 2 shown in Figs. 25–28. The values of the security of supply parameters at the end of the simulation (T_{max}) are summarised in Tables 6 & 7. The ENS for the gas system is reduced by more than 35 [%] and for the electricity system by almost 48 [%]. In addition, the SVT for both systems is increased to unlimited, since the total PENS for case 2 is always lower than the survival time tolerance of 1 [%]. Moreover, the TSP for the gas system is reduced by almost 30 [%] and for the electricity system by more than 13 [%]. Finally, the ENSTSP for both systems is reduced by roughly 26 [%]. Therefore, we can conclude that the countermeasure deployed in the gas system reduced the impact of the disruption triggered in compressor station CS.1 on security of supply in the combined gas and electric power system. Moreover, the countermeasure was more effective for the electricity network than for the gas network, even though, it was deployed in the gas network.

5. Conclusion

In this paper, we presented a novel quasi-dynamic simulation model for assessing security of supply in interconnected gas and electric transmission networks. The model consists of a transient hydraulic model for the gas system, which includes sub models of all important facilities and an extended ED for the electric power system, which contains a model for dispatchable loads and considers time transitional constraints such as the ramp rate and the start-up time of generation units. The models for the individual energy systems were combined through coupling equations describing the power supply to EDCSs and LNG terminals and the fuel gas offtake for power generation in GFPPs. The resulting system of equations describing the state change of the combined system between two consecutive time steps is solved iteratively by a sequential linearisation method, which updates the boundary conditions expressed by the coupling equations at each iteration step. In order to quantify the impact of contingencies on security of supply, we proposed five security of supply parameters, namely, (1) the energy not supplied, (2) the percentage of energy not supplied, (3) the survival time, (4) the time span of energy not supplied, and (5) the energy not supplied per time span.

Table 6
Summary of results for security of supply parameters for gas network.

GNET	$ENS(T_{max})$ [GW h]	$PENS(T_{max})$ [%]	$TSP(T_{max})$ [h]	$ENSTSP(T_{max})$ [MW]	$SVT(1[\%])$ [h]
Case 1	2.04	0.93	3.75	543.09	8
Case 2	1.31	0.60	3.25	403.23	–
Δ	−35.68 [%]	−35.48 [%]	−13.33 [%]	−25.75 [%]	–

Table 7
Summary of results for security of supply parameters for electric network.

ENET	$ENS(T_{max})$ [GW h]	$PENS(T_{max})$ [%]	$TSP(T_{max})$ [h]	$ENSTSP(T_{max})$ [MW]	$SVT(1[\%])$ [h]
Case1	0.09	1.26	6.30	14.02	6
Case2	0.05	0.66	4.45	10.41	–
Δ	−47.57 [%]	−47.62[%]	−29.37[%]	−25.76[%]	–

The security of supply parameters together with the algorithm for the combined energy system were implemented into a novel simulation software named *SAInt*, the first published simulation tool that allows the combined simulation of interconnected gas and electric power systems in a single time frame and simulation environment. The capabilities of the combined model and the functionality of the software tool were demonstrated in a case study of a sample combined gas and electric power system. The case studies were composed of three scenarios with supply disruptions triggered by the loss of wind power generation in the electric network (in all three cases 0, 1 & 2) and loss of gas compression and interruption of gas flow at a major compressor station (in case 1 and 2). In case 0 the loss of wind power generation is compensated by a backup GFPP, however, due to the start-up time limits, which causes a short delay in power generation from GFPPs after the loss of wind power generation, some power system loads are curtailed, in order to balance the reduced generation capacity. The curtailment of the power system loads was enabled by the dispatchable load model added to the basic ED. In case 1, the disruption in a compressor station affected gas offtake stations in the gas system and active power demand at load buses in the electric power system. The disruption caused the nodal gas pressure at the GFPP node and the linepack in the hydraulic area downstream the disrupted compressor station to fall below the threshold for starting-up and operating the GFPP. Thus, the start-up of the reserve GFPP to backup the loss of wind power generation is delayed a couple of hours. During this time period the generation capacity in the electric network was insufficient to balance the scheduled or expected power system loads. Thus, the loads at a number of power system buses were curtailed based on a priority factor assigned to each load bus, in order to balance supply and demand in the electric network. Finally, in the last case, we demonstrated how a countermeasure can be implemented to mitigate the impact of the disruption triggered in the compressor station and how the developed security of supply parameters can be utilised to evaluate the effectiveness of this countermeasure. The countermeasure consisted of increasing the withdrawal rate from a neighbouring UGS facility to full withdrawal capacity by setting the pressure control set point of the facility to maximum operating pipeline pressure if the linepack in the affected hydraulic area goes below a certain threshold. The results for case 2 show that the countermeasure helped mitigate the impact of the disruption on security of supply in both networks, since all security of supply parameters were significantly reduced. Remarkably, the countermeasure had a stronger effect on the electric power system than on the gas system, though it was deployed in the gas system.

In summary, the case study demonstrate the very detailed level of information that can be obtained from the presented combined model implemented into *SAInt*. Due to the size of the paper, we limited the discussion to the most important observations, however, there are many more observations that can be analysed further using the supplementary data added to this paper. The type of information provided in this paper, cannot be obtained by a steady state approach for the gas system or by the co-simulation approach adopted in previous scientific papers, due to their limitations. The provided information cannot only be used to analyse the propagation of contingencies, but also to develop and test strategies to react to contingencies, such as those described in the preventive action and emergency plan postulated in Regulation 994/2010 [31]. This may help gas and power TSOs, energy research institutes, policy makers, such as, competent authorities of EU-Member States, regulatory agencies etc. to take the right decisions on how to increase the resilience and security of supply in critical energy infrastructures. Furthermore, the security of supply parameters developed in this paper, can be used for further analysis of gas and electric power networks, such as sensitivity analysis, risk assessment or Monte Carlo simulation.

In the coming future, we intend to extend the simulation tool by a heat dynamics and gas quality tracking model, which will allow a better estimation of linepack and an impact assessment of hydrogen and/or SNG injections into the gas system by P2G facilities.

Acknowledgment

This work has been developed within the framework of the European Program for Critical Infrastructure Protection (EPCIP) of the European Commission. We would like to thank the reviewers for their comments, which have improved the quality of the paper. We would also like to express our gratitude to Dr. Tom van der Hoeven for the productive discussions and suggestions, which have improved the presented simulation tool.

Appendix A. Primal dual interior point method

The extended ED model is solved with the Primal Dual Interior Point Method (PDIPM) described in [41,48–50] by applying the Karush-Kuhn-Tucker (KKT) optimality condition to the Lagrangian function of the following augmented ED:

$$\min_{\mathbf{X},\mathbf{Z}} \quad f(\mathbf{X},\mathbf{Z}) = \sum_{i=1}^{N_g} f_i(P_{G,i}) - \sum_{i=1}^{N_b} f_i(P_{D,i}) - \gamma \sum_{i=1}^{N_{iq}} \ln(Z_i) \tag{A.1}$$

$$s.t. \quad \mathbf{G}(\mathbf{X}) = \mathbf{0},\ \mathbf{H}(\mathbf{X}) + \mathbf{Z} = \mathbf{0}, \mathbf{Z} > \mathbf{0} \tag{A.2}$$

where a set of positive slack variables $\mathbf{Z}$ is added to the set of inequality constraints and for each slack variable Z_i a logarithmic barrier function is subtracted from the cost function. The resulting Lagrangian function of the augmented ED yields:

$$L(\mathbf{X},\mathbf{Z},\lambda,\mu) = f(\mathbf{X},\mathbf{Z}) + \boldsymbol{\lambda}^T \cdot \mathbf{G}(\mathbf{X}) + \boldsymbol{\mu}^T \cdot [\mathbf{H}(\mathbf{X}) + \mathbf{Z}] \tag{A.3}$$

where λ and μ are the vector of Lagrange multipliers for the set of equality $\mathbf{G}(\mathbf{X})$ and inequality $\mathbf{H}(\mathbf{X})$ constraints, respectively. The optimal solution of the augmented ED must fulfil the first order optimality conditions (KKT-conditions):

$$\mathbf{F}(\mathbf{X},\mathbf{Z},\lambda,\mu) = \left[L_X, L_Z, L_\lambda, L_\mu\right]^T = \mathbf{0} \tag{A.4}$$

$$L_X = \frac{\partial L}{\partial \mathbf{X}},\ L_Z = \frac{\partial L}{\partial \mathbf{Z}},\ L_\lambda = \frac{\partial L}{\partial \boldsymbol{\lambda}},\ L_\mu = \frac{\partial L}{\partial \boldsymbol{\mu}} \tag{A.5}$$

$$\mu > \mathbf{0}, \mathbf{Z} > \mathbf{0} \tag{A.6}$$

which yields a non-linear equation system eq. (A.4) that can be solved for the solution variables $\mathbf{W} = [\mathbf{X},\mathbf{Z},\lambda,\boldsymbol{\mu}]^T$ using a Newton-Raphson approach

$$-\mathbf{F}^k = \left.\frac{\partial \mathbf{F}}{\partial \mathbf{W}}\right|^k \cdot \Delta\mathbf{W} \tag{A.7}$$

where the Newton updates for the primal $(\mathbf{X},\mathbf{Z})$ and dual $(\boldsymbol{\lambda},\boldsymbol{\mu})$ variables are truncated as follows, in order to maintain feasibility of the solution:

$$\mathbf{X}^{k+1} = \mathbf{X}^k + \alpha_p \cdot \Delta\mathbf{X},\ \mathbf{Z}^{k+1} = \mathbf{Z}^k + \alpha_p \cdot \Delta\mathbf{Z} \tag{A.8}$$

$$\boldsymbol{\lambda}^{k+1} = \boldsymbol{\lambda}^k + \alpha_d \cdot \Delta\boldsymbol{\lambda},\ \boldsymbol{\mu}^{k+1} = \boldsymbol{\mu}^k + \alpha_d \cdot \Delta\boldsymbol{\mu} \tag{A.9}$$

with

$$\alpha_p = \min\left(\zeta \cdot \min_{\Delta Z_i<0}\left(-\frac{Z_i}{\Delta Z_i}\right), 1\right),\ \alpha_d = \min\left(\zeta \cdot \min_{\Delta \mu_i<0}\left(-\frac{\mu_i}{\Delta \mu_i}\right), 1\right) \tag{A.10}$$

$$i = 1 \ldots N_{iq},\ 0.9 \leqslant \zeta \leqslant 1 \tag{A.11}$$

The optimal solution obtained for the augmented ED coincides with the optimal solution of the initial extended ED if the perturbation factor γ converges to zero during the iterative solution process. Thus, at each Newton step k the perturbation factor γ is modified using the average primal dual distance as follows:

$$\gamma = \sigma\left(\frac{\mu^T \cdot \mathbf{Z}}{N_{iq}}\right), 0 \leqslant \sigma \leqslant 1 \tag{A.12}$$

The Newton-Raphson iterations are completed successfully, if the infinity norm of the residual vector $\mathbf{F}^k$ and the perturbation factor γ are below a specified tolerance ϵ_f and ϵ_γ, respectively. The process is aborted if after a specified number of iterations k_{max} a converged solution is not reached. The presented PDIPM is designed for solving large scale problems with reasonable computation times [41], however, the method belongs to the class of Newton methods, which are known to be not globally convergent, i.e. convergence depends on the initial guess for the solution variables. However, results show good convergence [41] if a flat start ($\delta_i = 0$ & $|U_i| = 1$) or an available solution from a previous time step is chosen as an initial guess, as it is done in the algorithm for the combined gas and electric power system simulation (see Fig. 4) explained in Section 2.3.

The presented PDIPM has been implemented into `SAInt` using the complex matrix notations for the derivatives of the Lagrangian function (see eq. (A.4)–(A.7)) given in [50]. The accuracy of the implemented model has been confirmed by benchmarking the results against the Matlab-based power system library MATPOWER [41]. The results of an AC-OPF simulation conducted with `SAInt` and MATPOWER for the sample electric network are attached as supplementary data to the electronic version of this paper (see Appendix D.4).

Appendix B. Data for sample gas and power network used in the case study

The gas and electric network data used for the case study are given in Tables B.8–B.14. The actual native input files used in `SAInt` for the computations are available in the electronic version of this paper and are explained further in Appendix D.1.

Table B.8
Input data for nodes in gas model.

Nr	ID	Type	X [–]	Y [–]	H [m]	p^{min} [bar-g]	p^{max} [bar-g]	Q^{max} [ksm^3/h]	I^{max} [Msm^3]
0	NO.0	CBI	−2.5	4.1	50	20	60	600	
1	NO.1		−0.1	2	100				
2	NO.2		−0.1	1.2	100				
3	NO.3		4.4	2	150				
4	NO.4	GFPP	−3.8	−2	125	30	60	500	
5	NO.5		5	2	150				
6	NO.6		−6	−2	110				
7	NO.7		0	−4.2	75				
8	NO.8	IND	5	−3	50	25	60	250	
9	NO.9		5	4	40				
10	NO.10	LNG	−7	−3	70	40	60	375	510
11	NO.11	CGS	−7	−1	300	20	60	400	
12	NO.12		0	−5	75				
13	NO.13		−1.5	−6.5	120				
14	NO.14	CGS	−0.1	−8.1	215	16	50	250	
15	NO.15	CGS	−3.1	−8.1	45	30	50	275	
16	NO.16	IND	4	5	50	25	50	240	
17	NO.17		5	−5	60				
18	NO.18	GFPP	5	−5.6	60	30	60		
19	NO.19		5	−7	170				
20	NO.20	CGS	4	−8.1	160	16			
21	NO.21	CBE	6	−8	150	30	60		
22	NO.22	UGS	7	−3	140	30	60	120	450
23	NO.23	GFPP	7	4	110	30	60		
24	NO.24	CGS	7	0.5	80	16	50		

Table B.9
Input data for pipelines in gas model.

ID	FrNr	ToNr	D [mm]	l [km]	k [mm]
Pl.0	0	1	900	100	0.012
Pl.1	1	3	900	80	0.012
Pl.2	2	4	600	50	0.01
Pl.3	4	6	300	20	0.02
Pl.4	6	11	300	10	0.0112
Pl.5	6	10	300	15	0.01
Pl.6	4	7	600	60	0.012
Pl.7	5	9	600	30	0.01
Pl.8	9	23	600	30	0.012
Pl.9	23	24	300	50	0.012
Pl.10	24	22	300	40	0.01
Pl.11	22	8	600	60	0.09
Pl.12	8	17	600	60	0.012
Pl.13	12	13	300	40	0.012
Pl.14	13	15	300	25	0.012
Pl.15	13	14	300	20	0.011
Pl.16	14	20	300	50	0.012
Pl.17	18	19	600	60	0.01
Pl.18	19	20	300	30	0.012
Pl.19	19	21	600	40	0.012
Pl.20	9	16	300	30	0.012
Pl.21	12	17	900	100	0.01
Pl.22	17	18	600	50	0.012

Table B.10
Input data for compressor stations.

ID	FrNr	ToNr	D [mm]	η_{ad} [–]	η_m [–]	f [–]
CS.0	1	2	600	0.78	0.9	1
CS.1	3	5	600	0.76	0.88	1
CS.2	7	12	600	0.79	0.91	1
ID	PI^{min} [bar-g]	PO^{max} [bar-g]	Π^{max} [–]	PWD^{max} [MW]	Q_{vol}^{max} [m^3/s]	Q^{max} [ksm^3/h]
CS.0	25	60	2.5	55	50	1000
CS.1	25	60	2	40	50	1500
CS.2	20	60	2.5	45	50	1000

Table B.11
Input data for electric power supply to LNG terminal.

Facility	ID	k_0 [MW]	k_1 $\left[\frac{MW}{sm^3/s}\right]$	k_2 $\left[\frac{MW}{(sm^3/s)^2}\right]$
LNG terminal	NO.10	5	0.208	−0.000723

Table B.12
Input data for buses in power network. Priority factor λ is chosen such that buses connected to LDSs are less likely to be affected by load shedding than buses connected to INDs and CBEs.

Nr	ID	BasekV [kV]	V_m^{min} [p.u.]	V_m^{max} [p.u.]	λ [−]	ϵ_{svt} [%]	X [−]	Y [−]
0	GEN.0	135	0.95	1.05	–	–	−27.6	1.3
1	GEN.1	135	0.95	1.1	–	–	−24.6	1.3
2	BUS.2	135	0.95	1.05	10	1	−27.6	−0.2
3	BUS.3	135	0.95	1.05	1	1	−24.6	−0.2
4	BUS.4	135	0.95	1.05	1	1	−21.5	1.3
5	BUS.5	135	0.95	1.05	1	1	−22	−0.3
6	BUS.6	135	0.95	1.05	10	1	−19	1.3
7	BUS.7	135	0.95	1.05	10	1	−19.6	−1
8	BUS.8	135	0.95	1.05	1	1	−22	−2.1
9	BUS.9	135	0.95	1.05	1	1	−18.9	−3.5
10	BUS.10	135	0.95	1.05	10	1	−23.2	−2.1
11	BUS.11	135	0.95	1.05	1	1	−24.6	−2.5
12	GEN.12	135	0.95	1.1	–	–	−27.6	−2.5
13	BUS.13	135	0.95	1.05	10	1	−26.7	−4.4
14	BUS.14	135	0.95	1.05	10	1	−24.6	−5.9
15	BUS.15	135	0.95	1.05	10	1	−23.3	−4.5
16	BUS.16	135	0.95	1.05	1	1	−21	−4.5
17	BUS.17	135	0.95	1.05	10	1	−23.3	−5.9
18	BUS.18	135	0.95	1.05	1	1	−21.9	−5.9
19	BUS.19	135	0.95	1.05	10	1	−20.6	−5.9
20	BUS.20	135	0.95	1.05	1	1	−17.5	−4.3
21	GEN.21	135	0.95	1.1	–	–	−18.9	−5.4
22	GEN.22	135	0.95	1.1	–	–	−24.6	−8.5
23	BUS.23	135	0.95	1.05	1	1	−22.1	−8.5
24	BUS.24	135	0.95	1.05	1	1	−19.7	−8.5
25	BUS.25	135	0.95	1.05	1	1	−17.7	−8.5
26	GEN.26	135	0.95	1.1	–	–	−16.4	−4.4
27	BUS.27	135	0.95	1.05	5	1	−18	0.4
28	BUS.28	135	0.95	1.05	5	1	−15.1	−3.8
29	BUS.29	135	0.95	1.05	5	1	−15.6	−4.9

Table B.13
Input data for transmission lines in power network.

ID	FrNr	ToNr	R [p.u.]	X [p.u.]	b [p.u.]	S^{max} [MVA]
LINE.0	0	1	0.02	0.06	0.03	100
LINE.1	0	2	0.05	0.19	0.02	100
LINE.2	1	3	0.06	0.17	0.02	100
LINE.3	2	3	0.01	0.04	0	100
LINE.4	1	4	0.05	0.2	0.02	100
LINE.5	1	5	0.06	0.18	0.02	100
LINE.6	3	5	0.01	0.04	0	100
LINE.7	4	6	0.05	0.12	0.01	100
LINE.8	5	6	0.03	0.08	0.01	100
LINE.9	5	7	0.01	0.04	0	100
LINE.10	5	8	0	0.21	0	100
LINE.11	5	9	0	0.56	0	100
LINE.12	8	10	0	0.21	0	100
LINE.13	8	9	0	0.11	0	100
LINE.14	3	11	0	0.26	0	100
LINE.15	11	12	0	0.14	0	100
LINE.16	11	13	0.12	0.26	0	100
LINE.17	11	14	0.07	0.13	0	100
LINE.18	11	15	0.09	0.2	0	100
LINE.19	13	14	0.22	0.2	0	100
LINE.20	15	16	0.08	0.19	0	100
LINE.21	14	17	0.11	0.22	0	100
LINE.22	17	18	0.06	0.13	0	100
LINE.23	18	19	0.03	0.07	0	100
LINE.24	9	19	0.09	0.21	0	100
LINE.25	9	16	0.03	0.08	0	100
LINE.26	9	20	0.03	0.07	0	100
LINE.27	9	21	0.07	0.15	0	100
LINE.28	20	21	0.01	0.02	0	100
LINE.29	14	22	0.1	0.2	0	100
LINE.30	21	23	0.12	0.18	0	100
LINE.31	22	23	0.13	0.27	0	100
LINE.32	23	24	0.19	0.33	0	100
LINE.33	24	25	0.25	0.38	0	100
LINE.34	24	26	0.11	0.21	0	100
LINE.35	27	26	0	0.4	0	100
LINE.36	26	28	0.22	0.42	0	100
LINE.37	26	29	0.32	0.6	0	100
LINE.38	28	29	0.24	0.45	0	100
LINE.39	7	27	0.06	0.2	0.02	100
LINE.40	5	27	0.02	0.06	0.01	100

Appendix C. Simulation results for combined steady state simulation

The results for the combined steady state simulation are given in Tables C.15–C.18.

Appendix D. Description of supplementary data available in the electronic version

All supplementary files are available in Appendix E. In the following sections, we give a description of the different files.

D.1. `SAInt` project files

The input files provided as supplementary data to the electronic version of this paper include all input data used for the network and for the case studies. All files are original `SAInt` input files and are provided in xml format. A `SAInt`- project is generally divided into the following four types of files:

(1) `SAInt` – Network files (with extensions ∗.net, ∗.enet):
Network files contain all topological information of the individual network and its static properties, which typically do not change in the course of a simulation (e.g. transmission line and pipeline properties). Each network in a project has its own file and the network type is expressed by its file extension (e.g. ∗.net for gas network, ∗.enet for electric network).

(2) `SAInt` – Scenario files (with extensions ∗.sce, ∗.esce):
For each network file, we can define an unlimited number of scenarios or cases, which include all boundary conditions, conditional expressions, load profiles etc. Each scenario file is associated to a network (file). The type of network a scenario is connected to is expressed by its file extension, analogous to the network file extensions (e.g. ∗.sce for gas network, ∗.esce for electric network).

(3) `SAInt` – State or condition files (with extensions ∗.con, ∗.econ):
The network and scenario files are both input files generated by `SAInt`. The state or condition files, in contrast, are result files generated after each simulation run. The state file contains the solution for all state variables for the terminal state of a simulation. It can be regarded as a snapshot of the network at the end of the simulation. The state file is needed as a initial state of the network for computing a (combined) dynamic simulation. Each state file is associated to a sce-

Table B.14
Input data for generation units in power model.

ID	P_G^{max} [MW]	P_G^{min} [MW]	Q_G^{max} [MVAr]	Q_G^{min} [MVAr]	ω_r [MW/min]	T_s^{min} [h]	T_s^{max} [h]
GEN.0	60	15	48	−36	3	2	4
GEN.1	100	25	80	−60	2.5	2	8
GEN.12	50	12.5	40	−30	7.5	1/4	1/2
GEN.21	60	15	48	−36	3	2	4
GEN.22	60	15	48	−36	3	3	20
GEN.26	115	28.75	92	−69	5.75	3	20

ID	c_0 [€]	c_1 $\left[\frac{€}{MW}\right]$	c_2 $\left[\frac{€}{MW^2}\right]$	α $\left[\frac{MJ}{kW\ h}\right]$	β $\left[\frac{MJ}{kW\ h\ MW}\right]$	γ $\left[\frac{MJ}{kW\ h\ MW^2}\right]$
GEN.0	65	3.75	0.06	22.3590	−0.5607	0.0047
GEN.1	55	1.125	0.01	–	–	–
GEN.12	60	4.5	0.04	56.0000	−1.8286	0.0183
GEN.21	50	3.75	0.06	22.3590	−0.5607	0.0047
GEN.22	55	1.05	0.003	–	–	–
GEN.26	30	1.1	0.01	–	–	–

Table C.15
Nodal control set points and results for initial combined steady state computation. Negative Q means gas supply, positive Q gas offtake.

ID	CTRL	CTRLV	Q [ksm³/h]	p [bar-g]
NO.0	PSET	50 [bar-g]	−531.877	50
NO.1	OFF		0	45.734
NO.2	OFF		0	60
NO.3	OFF		0	45.319
NO.4	QSET	6.118 [ksm³/h]	6.118	52.325
NO.5	OFF		0	60
NO.6	OFF		0	56.013
NO.7	OFF		0	36.694
NO.8	QSET	250 [ksm³/h]	250	55.364
NO.9	OFF		0	60.078
NO.10	PSET	60 [bar-g]	−87.931	60
NO.11	QSET	20 [ksm³/h]	20	54.986
NO.12	OFF		0	60
NO.13	OFF		0	52.674
NO.14	QSET	40 [ksm³/h]	40	50.93
NO.15	QSET	30 [ksm³/h]	30	52.1
NO.16	QSET	50 [ksm³/h]	50	57.483
NO.17	OFF		0	58.319
NO.18	QSET	6.403 [ksm³/h]	6.403	56.994
NO.19	OFF		0	54.99
NO.20	QSET	60 [ksm³/h]	60	51.155
NO.21	QSET	100 [ksm³/h]	100	54.653
NO.22	PSET	55 [bar-g]	−92.713	55
NO.23	QSET	0 [ksm³/h]	0	59.538
NO.24	QSET	150 [ksm³/h]	150	47.908

Table C.16
Compressor stations control set points and results for initial combined steady state computation.

ID	CTRL	CTRLV	Q [ksm³/h]	PI [bar-g]	PO [bar-g]	PWD [MW]
CS.0	POSET	60 [bar-g]	401.667	45.734	60	4.171
CS.1	POSET	60 [bar-g]	130.21	45.319	60	1.47
CS.2	POSET	60 [bar-g]	463.48	36.694	60	8.886

nario (file). The type of network a state is connected to is expressed by its file extension, analogous to the network file extensions (e.g. ∗.con for gas network state file, ∗.econ for electric network state file).

(4) and `SAInt` – Solution files (with extensions ∗.sol, ∗.esol): The simulation results for a scenario are saved in a solution file. The result of a dynamic simulation is a sequence of network states (snapshots) for each simulation time step. To limit the size of the solution files the result for each state contains only fundamental parameters that cannot be calculated or derived from a combination of other parameters such as nodal gas pressure, voltage angle and magnitude. The type of network a solution file is connected to is expressed by its file extension, analogous to the network file extensions (e.g. ∗.sol for gas network solution file, ∗.esol for electric network solution file).

In the following, we list all network, scenario, state and solution files used for the case study and provided as supplementary data and give a short description of their content:

Table C.17
Results for power system buses for initial combined steady state simulation.

ID	δ [°]	V_m [kV]	V_m [p.u.]	PD [MW]	PDGAS [MW]	QD [MVAr]
GEN.0	0	141.75	1.05	0	0	0
GEN.1	0.115	142.543	1.056	0	0	0
BUS.2	−2.359	138.707	1.027	5	0	1.2
BUS.3	−2.762	138.185	1.024	0	0	0
BUS.4	−1.87	139.741	1.035	0	0	0
BUS.5	−3.224	137.514	1.019	0	0	0
BUS.6	−2.999	137.325	1.017	12	4.171	10.9
BUS.7	−3.578	136.082	1.008	25	1.47	30
BUS.8	−6.962	137.015	1.015	0	0	0
BUS.9	−7.457	137.343	1.017	0	0	0
BUS.10	−9.78	136.358	1.01	24	0	1.75
BUS.11	−7.241	136.759	1.013	0	0	0
GEN.12	−7.241	136.759	1.013	0	0	0
BUS.13	−9.616	132.592	0.982	24	8.053	1.6
BUS.14	−7.707	136.635	1.012	7	8.886	2.5
BUS.15	−8.11	135.577	1.004	9	0	1.8
BUS.16	−8.056	135.955	1.007	15	0	5.8
BUS.17	−9.796	133.445	0.988	10	0	0.9
BUS.18	−10.337	132.718	0.983	8	0	3.4
BUS.19	−10.359	133.009	0.985	25	0	0.7
BUS.20	−7.151	138.57	1.026	16	0	11.2
GEN.21	−6.959	139.448	1.033	0	0	0
GEN.22	−3.397	144.369	1.069	0	0	0
BUS.23	−5.347	141.75	1.05	0	0	0
BUS.24	−4.871	141.75	1.05	0	0	0
BUS.25	−11.06	129.103	0.956	30	0	2.3
GEN.26	−1.528	148.206	1.098	0	0	0
BUS.27	−3.251	138.546	1.026	0	0	0
BUS.28	−9.218	135.13	1.001	30	0	0.9
BUS.29	−10.654	132.639	0.983	35	0	1.9

Table C.18
Results for power system generation units for initial combined steady state simulation.

ID	PG [MW]	QG [MVAr]	Q [ksm^3/h]	COST [€]	HR [MJ/kW h]	η_T [–]
GEN.0	18.63	−4.549	6.118	155.686	13.535	0.266
GEN.1	100	28.022	0	267.5	–	–
GEN.12	0	0	0	60	–	–
GEN.21	20.676	27.522	6.403	153.183	12.764	0.282
GEN.22	60	10.36	0	128.8	–	–
GEN.26	115	40.635	0	288.75	–	–

(1) GNET25.net – Gas network file for sample 25 Node gas network
(2) ENET30.enet – Electric network file for sample 30 Bus IEEE power network
(3) CMBSTEOPF.sce – Gas network scenario file for the combined steady state scenario
(4) CMBSTEOPF.esce – Electric network scenario file for the combined steady state scenario
(5) CMBSTEOPF.con – Gas network state file for the combined steady state scenario
(6) CMBSTEOPF.econ – Electric network state file for the combined steady state scenario
(7) Case0.sce – Gas network scenario file for the combined dynamic scenario for case 0
(8) Case0.esce – Electric network scenario file for the combined dynamic scenario for case 0
(9) Case0.sol – Gas network solution file for the combined dynamic scenario for case 0
(10) Case0.esol – Electric network solution file for the combined dynamic scenario for case 0
(11) Case1.sce – Gas network scenario file for the combined dynamic scenario for case 1
(12) Case1.esce – Electric network scenario file for the combined dynamic scenario for case 1
(13) Case1.sol – Gas network solution file for the combined dynamic scenario for case 1
(14) Case1.esol – Electric network scenario file for the combined dynamic scenario for case 1
(15) Case2.sce – Gas network scenario file for the combined dynamic scenario for case 2
(16) Case2.esce – Electric network scenario file for the combined dynamic scenario for case 2
(17) Case2.sol – Gas network solution file for the combined dynamic scenario for case 2
(18) Case2.esol – Electric network solution file for the combined dynamic scenario for case 2

D.2. Animation videos for the case studies generated with `SAInt`

The animation videos for the three cases were generated by `SAInt` and are provided as animated GIF-files, which can be played in any web browser. The videos show the time evolution of the state variables, the direction of gas flow and electric current, and the state changes of controlled facilities in the gas and power system. The description of the different symbols in the video are given in the caption of Fig. 8. The digital clock in the bottom mid-section indicates the current simulation time.

D.3. Simulation protocol for the case studies generated with SAInt

The simulation protocols were exported from the SAInt-log window and contain information on the total simulation time, the number of iterations in the successive linearisation loop, time integration loop, and the CCH-loop (as explained in Section 2.3 and the flow chart depicted in Fig. 4), the residual for the gas and power system equations and the residual for the value of the coupling equations for the last two consecutive steps of the successive linearisation loop. Furthermore, the protocol contains a number of actions implemented by the solver to avoid constraints violations in the gas network.

D.4. Comparison between SAInt & MATPOWER [50] for AC-OPF

The comparison between SAInt and MATPOWER were conducted for a single AC-OPF simulation for the sample electric network used in the case study. The input data and results obtained with SAInt are included in the Excel file ComparisonSAInt.xls while the ones for MATPOWER are given in ComparisonMatpowerResult.log. A comparison of the results confirms the accuracy of the AC-OPF model implemented into SAInt.

Appendix E. Supplementary material

Supplementary data associated with this article can be found, in the online version, at http://dx.doi.org/10.1016/j.apenergy.2017.05.142.

References

[1] Pearson I, Zeniewski P, Gracceva F, Zastera P, McGlade C, Sorrell S. Unconventional gas: potential energy market impacts in the European Union, Technical Report, JRC scientific and policy reports EUR 25305 EN; 2012.
[2] Judson N. Interdependence of the electricity generation system and the natural gas system and implications for energy security. Technical Report. Massachusetts Institute of Technology Lincoln Laboratory; 2013.
[3] Greenblatt JB. Opportunities for efficiency improvements in the u.s. natural gas transmission, storage and distribution system; 2015.
[4] Clegg S, Mancarella P. Storing renewables in the gas network: modelling of power-to-gas seasonal storage flexibility in low-carbon power systems. IET Gener Transm Distrib 2016.
[5] Clegg S, Mancarella P. Integrated modeling and assessment of the operational impact of power-to-gas (p2g) on electrical and gas transmission networks. IEEE Trans Sustain Energy 2015;6:1234–44.
[6] Clegg S, Mancarella P. Integrated electrical and gas network flexibility assessment in low-carbon multi-energy systems. IEEE Trans Sustain Energy 2016;7(2):718–31.
[7] Devlin J, Li K, Higgins P, Foley A. A multi vector energy analysis for interconnected power and gas systems. Appl Energy 2016.
[8] Cakir Erdener B, Pambour KA, Lavin RB, Dengiz B. An integrated simulation model for analysing electricity and gas systems. Int J Electric Power Energy Syst 2014;61:410–20.
[9] Zhang X, Che L, Shahidehpour M. Impact of natural gas system on short-term scheduling with volatile renewable energy. In: 2015 IEEE power energy society general meeting. p. 1–5. http://dx.doi.org/10.1109/PESGM.2015.7285633.
[10] Sardou IG, Khodayar ME, Ameli M. Coordinated operation of natural gas and electricity networks with microgrid aggregators. IEEE Trans Smart Grid 2016;PP. pp. 1–1.
[11] Alabdulwahab A, Abusorrah A, Zhang X, Shahidehpour M. Coordination of interdependent natural gas and electricity infrastructures for firming the variability of wind energy in stochastic day-ahead scheduling. IEEE Trans Sustain Energy 2015;6:606–15.
[12] Liu C, Shahidehpour M, Fu Y, Li Z. Security-constrained unit commitment with natural gas transmission constraints. IEEE Trans Power Syst 2009.
[13] Zlotnik A, Chertkov M, Carter R, Hollis A, Daniels A, Backhaus S. Using power grid schedules in dynamic optimization of gas pipelines. In: Pipeline simulation interest group.
[14] Pambour KA, Cakir Erdener B, Bolado-Lavin R, Dijkema GPJ. Development of a simulation framework for analyzing security of supply in integrated gas and electric power systems. Appl Sci 2017.
[15] Pambour KA, Cakir Erdener B, Bolado-Lavin R, Dijkema GPJ. An integrated simulation tool for analyzing the operation and interdependency of natural gas and electric power systems. In: Pipeline Simulation Interest Group (PSIG) conference 2016. , <https://www.onepetro.org/conference-paper/PSIG-1609>.
[16] Zeng Q, Fang J, Li J, Chen Z. Steady-state analysis of the integrated natural gas and electric power system with bi-directional energy conversion. Appl Energy 2016.
[17] Chen S, Wei Z, Sun G, Cheung KW, Sun Y. Multi-linear probabilistic energy flow analysis of integrated electrical and natural-gas systems. IEEE Trans Power Syst 2016;PP. pp. 1–1.
[18] Zlotnik A, Roald L, Backhaus S, Chertkov M, Andersson G. Coordinated scheduling for interdependent electric power and natural gas infrastructures. IEEE Trans Power Syst 2016;PP. pp. 1–1.
[19] Badakhshan S, Kazemi M, Ehsan M. Security constrained unit commitment with flexibility in natural gas transmission delivery. J Nat Gas Sci Eng 2015;27 (Part 2):632–40.
[20] Zhang X, Che L, Shahidehpour M. Long-term expansion planning of integrated electricity and natural gas transportation infrastructures. In: 2015 IEEE power energy society general meeting. p. 1–5. http://dx.doi.org/10.1109/PESGM.2015.7286218.
[21] Liu C, Shahidehpour M, Wang J. Application of augmented lagrangian relaxation to coordinated scheduling of interdependent hydrothermal power and natural gas systems. IET Gener Transm Distrib 2010;4:1314–25.
[22] Li G, Zhang R, Jiang T, Chen H, Bai L, Li X. Security-constrained bi-level economic dispatch model for integrated natural gas and electricity systems considering wind power and power-to-gas process. Appl Energy 2016.
[23] Qiu J, Dong ZY, Zhao JH, Xu Y, Zheng Y, Li C, et al. Multi-stage flexible expansion co-planning under uncertainties in a combined electricity and gas market. IEEE Trans Power Syst 2015;30:2119–29.
[24] Bai L, Li F, Cui H, Jiang T, Sun H, Zhu J. Interval optimization based operating strategy for gas-electricity integrated energy systems considering demand response and wind uncertainty. Appl Energy 2016;167:270–9.
[25] Zhang X, Shahidehpour M, Alabdulwahab A, Abusorrah A. Hourly electricity demand response in the stochastic day-ahead scheduling of coordinated electricity and natural gas networks. IEEE Trans Power Syst 2016;31:592–601.
[26] Asif U, Jirutitijaroen P. An optimization model for risk management in natural gas supply and energy portfolio of a generation company. In: Proceedings of TENCON 2009-2009 IEEE region 10 conference.
[27] Chaudry M, Jenkins N, Strbac G. Multi-time periode combined gas and electricity network optimisation. Electr Power Syst Res 2008;78:1265–79.
[28] Chiang N-Y, Zavala VM. Large-scale optimal control of interconnected natural gas and electrical transmission systems. Appl Energy 2016;168:226–35.
[29] Pambour KA, Bolado-Lavin R, Dijkema GP. SAInt – A simulation tool for analysing the consequences of natural gas supply disruptions. In: Pipeline Technology Conference (PTC) 2016. <http://www.pipeline-conference.com/abstracts/saint-simulation-tool-analyzing-consequences-gas-supply-disruptions>.
[30] Andersson G. Modelling and analysis of electric power systems, Lecture 227-0526-00, ITET ETH Zurich; 2008.
[31] European Union, Regulation (EU) No 994/2010 of the european parliament and the council of 20 october 2010 concerning measures to safeguard security of gas supply and repealing council directive 2004/67/ec, Official Journal of the Europian Union; 2010. <http://eur-lex.europa.eu/legal-content/EN/TXT/PDF/?uri=CELEX:32010R0994&from=EN> [May 16, 2017].
[32] Osiadacz AJ, Chaczykowski M. Comparison of isothermal and non-isothermal pipeline gas flow models. Chem Eng J 2001;81:41–51.
[33] Osiadacz AJ. Simulation and analysis of gas networks. E. & F.N. SPON; 1987.
[34] Herrán-González A, Cruz JDL, Andrés-Toro BD, Risco-Martín J. Modeling and simulation of a gas distribution pipeline network. Appl Math Model 2009;33:1584–600.
[35] Herty M. Modeling, simulation and optimization of gas networks with compressors. Networks Hetrogeneous Media© Am Inst Math Sci 2007;2:81–7.
[36] Woldeyohannes AD, Abd Majid MA. Simulation model for natural gas transmission pipeline network system. Simul Model Pract Theory – Elsevier B.V. 2011;19:196–212.
[37] Dorao C, Fernandino M. Simulation of transients in natural gas pipelines. J Nat Gas Sci Eng 2011;3:349–55.
[38] Pambour KA, Bolado-Lavin R, Dijkema GP. An integrated transient model for simulating the operation of natural gas transport systems. J Nat Gas Sci Eng 2016;28:672–90.
[39] Králik J. Dynamic modeling of large-scale networks with application to gas distribution, Studies in automation and control. Elsevier; 1988, <https://books.google.de/books?id=FFk2AQAAIAAJ>.
[40] Carter R, Backhaus S, Hollis A, Zlotnik A, Chertkov M, Giacomoni A, et al. Impact of regulatory change to coordinate gas pipelines and power systems. In: Pipeline simulation interest group.
[41] Zimmerman RD, Murillo-Sanchez CE, Thomas RJ. Matpower: steady-state operations, planning and analysis tools for power systems research and education. IEEE Trans Power Syst 2011;26:12–9.
[42] Brouwer AS, van den Broek M, Seebregts A, Faaij A. Operational flexibility and economics of power plants in future low-carbon power systems. Appl Energy 2015;156:107–28.
[43] Martinez-Mares A, Fuerte-Esquivel CR. A unified gas and power flow analysis in natural gas and electricity coupled networks. IEEE Trans Power Syst 2012;27.
[44] Cerbe G. Grundlagen der Gastechnik. HANSER; 2008.
[45] Aoki I, Kikkawa Y. LNG plant combined with power plant. Chiyoda Corporation; 2016.
[46] Duff IS, Erisman AM, Reid JK. Direct Methods for Sparse Matrices. New York, NY, USA: Oxford University Press, Inc.; 1986.

[47] Soman SA, Khaparde SA, Pandit S. Computational methods for large sparse power systems analysis. Springer; 2002.
[48] Wang H. On the computation and application of multi-period security-constrained optimal power flow for real-time electricity market operations [Ph.D. thesis]. Cornell University; 2007.
[49] Zimmerman RD, Murrillo-Sanchez CE. Matpower 5.1 User's Manual, Power Systems Engineering Research Center (Pserc); 2015.
[50] Zimmerman RD. AC power flows, generalized opf costs and their derivatives using complex matrix notation – matpower technical note 2, Power Systems Engineering Research Center (Pserc); 2011.